

# APPLICATION OF A NEAR-OPTIMAL FEEDBACK GUIDANCE ALGORITHM TO SPACECRAFT IN DYNAMICALLY COMPLEX ENVIRONMENTS

Joel R. Mueting

---

Copyright © Joel R. Mueting 2017

A Thesis Submitted to the Faculty of the  
SYSTEMS AND INDUSTRIAL ENGINEERING  
DEPARTMENT

In Partial Fulfillment of the Requirements For the Degree of

MASTER OF SCIENCE  
WITH A MAJOR IN SYSTEMS ENGINEERING

In the Graduate College of  
THE UNIVERSITY OF ARIZONA

**2017**

## STATEMENT BY AUTHOR

The thesis titled *Application of a Near-Optimal Feedback Guidance Algorithm to Spacecraft in Dynamically Complex Environments* prepared by Joel Mueting has been submitted in partial fulfillment of requirements for a master's degree at the University of Arizona and is deposited in the University Library to be made available to borrowers under rules of the Library.

Brief quotations from this thesis are allowable without special permission, provided that an accurate acknowledgement of the source is made. Requests for permission for extended quotation from or reproduction of this manuscript in whole or in part may be granted by the head of the major department or the Dean of the Graduate College when in his or her judgment the proposed use of the material is in the interests of scholarship. In all other instances, however, permission must be obtained from the author.

SIGNED: Joel Mueting

## APPROVAL BY THESIS DIRECTOR

This thesis has been approved on the date shown below:

---

*Dr. Roberto Furfaro*  
*Assistant Professor in Systems & Industrial Engineering*

*Defense date*  
*12/16/2016*

# Acknowledgments

I would like to thank Dr. Roberto Furfaro for all of the guidance and challenging opportunities he has provided for me during my graduate studies. I would also like to thank my family and my partner Tyler for their unwavering support over the past few years.

# Abstract

A near-optimal feedback guidance algorithm is applied to several different applications in the Circular-Restricted Three Body Problem and in proximity operations in LEO modeled by Keplerian motion. In both scenarios gravitational perturbations are introduced in order to assess the algorithm's robustness. Two forms of the guidance algorithm are studied: a zero-effort miss/zero-effort velocity feedback control law and a zero-effort miss/zero-effort velocity feedback control law augmented with a sliding mode. Both guidance laws have previously been applied to the problems of planetary landing, asteroid intercept, and close-proximity maneuvers near an asteroid. This study is motivated by the growing interest in spacecraft autonomy for proximity operations and in cases where a high frequency of open-loop commanded maneuvers is not practical. Results demonstrate that nominal zero-effort miss/zero-effort velocity feedback guidance is suboptimal in all test cases, but performance can be improved through the addition of waypoints and tuning of guidance law parameters. Additionally, the application of a sliding-mode is shown to overcome limitations introduced by gravitational perturbations in some instances.

# Contents

<b>1</b>	<b>Introduction</b>	<b>8</b>
1.0.1	Problem Definition . . . . .	15
1.0.2	Outline . . . . .	15
1.1	Circular Restricted Three-Body Problem . . . . .	16
1.1.1	Equations of Motion . . . . .	16
1.1.2	Libration Points . . . . .	24
1.1.3	Libration Point Orbits . . . . .	26
1.2	Spacecraft Formation Flight . . . . .	30
1.2.1	General Equations of Relative Motion . . . . .	30
1.2.2	Linearized Relative Equations of Motion and the Clohessy- Wiltshire-Hill Equations . . . . .	35
<b>2</b>	<b>Guidance Problem Development</b>	<b>38</b>
2.1	Zero-Effort Miss/Zero-Effort Velocity . . . . .	38
2.2	Optimal Guidance Law . . . . .	40
2.3	Sliding Guidance Development . . . . .	45
2.3.1	Sliding Mode Control Theory . . . . .	45
2.3.2	Design of Optimal Sliding Guidance (OSG) . . . . .	48
<b>3</b>	<b>Methods</b>	<b>52</b>
3.1	Halo Orbit Initial Conditions . . . . .	52

3.2	Halo Orbit Perturbations . . . . .	55
3.3	Implementation of Relative Motion Equations . . . . .	56
3.4	Geospatial Perturbations . . . . .	57
3.5	Control Algorithm . . . . .	59
3.5.1	Basic Guidance Algorithm . . . . .	59
3.5.2	Stationkeeping Algorithm . . . . .	60
<b>4</b>	<b>Results</b>	<b>63</b>
4.1	Circular-Restricted Three Body Problem . . . . .	63
4.1.1	Halo Orbit Station-keeping . . . . .	63
4.1.2	Halo Orbit Transfer . . . . .	68
4.2	Formation Flight in Low Earth Orbit . . . . .	69
<b>5</b>	<b>Conclusions</b>	<b>75</b>

# List of Figures

1.1	Three Body Problem in Inertial Frame . . . . .	17
1.2	Three Body Problem Rotating Frame . . . . .	19
1.3	Geometric Layout of Libration Points in the $x, y$ Plane . . . . .	24
1.4	Example Halo Orbit Near Earth-Moon L2 . . . . .	27
1.5	Chief-Deputy Relative Motion Illustration . . . . .	31
3.1	Halo Orbit Stationkeeping Guidance Algorithm . . . . .	61
4.1	Application of OGL as Station-Keeping Solution in Bicircular-Restricted Four Body Problem . . . . .	64
4.2	Extended station-keeping case in the CRTBP . . . . .	65
4.3	Parametric Study of OSG Applied to Station-keeping in the Bicircular Restricted Four-Body model . . . . .	67
4.4	OSG Tracking to Optimal Transfer Trajectory Between Two Halo Orbits	68
4.5	Performance of ZEM/ZEV Feedback Guidance vs. $D_r/D_v$ Feedback Guidance in CHW Model . . . . .	71
4.6	Comparison between two optimal solutions computed offline and OGL	72
4.7	Parametric Study of OSG in LERM Model . . . . .	73
4.8	Performance of OGL vs. OSG in $J_2$ -Perturbed Restricted Two-Body Problem . . . . .	74

# List of Tables

4.1	Waypoint Study in Bicircular Restricted Four-Body Problem . . . . .	66
4.2	Effect of OSG Waypoints on Optimal Transfer Trajectory . . . . .	69
4.3	Initial Conditions for CHW model . . . . .	70
4.4	Fuel-Optimal Parameters in LERM Parametric Study . . . . .	72
4.5	Initial Conditions for J2-Perturbed Model . . . . .	73

# Introduction

Over the past decade, an increased focus has been placed on spacecraft automation for both deep space and earth-orbiting missions. In highly uncertain environments in which an operational command cadence to a spacecraft may not be frequent enough to achieve a mission objective, it is desirable to employ a robust guidance controller to ensure that targeted flight conditions are met. More importantly, it is desirable for any such controller to optimize guided flight such that fuel expenditure is minimized. Such situations, for example, can include spacecraft in dynamically complex environments and proximity operations between spacecraft. Both of which are cases that have been the subject of increased study in recent years.

In this paper, the performance of a zero-effort miss, zero-effort velocity feedback guidance algorithm that has been shown to perform optimally in the case of planetary landing is measured in more dynamically complex environments. Two separate environments are chosen for this purpose: operations in a periodic, unstable orbit in the Earth-Moon circular restricted three-body system and the dynamics of spacecraft flight formation in low earth orbit. The optimal feedback guidance algorithm is the analytical result of an optimal control problem formulated to minimize the commanded thrust acceleration of a spacecraft in the powered descent phase of a planetary landing.[2, 3] Theoretically this control law is only optimal in cases of highly simpli-

fied conditions such as operating very near a planetary surface where gravity can be assumed to be constant and with no perturbing forces such as wind resistance. However, recent research has shown that the zero-effort miss, zero-effort velocity feedback control law can perform near-optimally in more perturbed dynamical environments [23, 24, 12, 26, 15].

The optimal guidance law (OGL) studied in this investigation was first derived by D’Souza in his paper *An Optimal Guidance Law for Planetary Landing*. D’Souza demonstrated that a closed-form analytical solution can be derived from an optimal control problem formulation that seeks to minimize commanded acceleration of a vehicle landing on the surface of a planet.[3] This analytical form is only accomplished, however, when simplifying assumptions are made. That is, the only forces acting on the landing vehicle are the commanded acceleration and the effect of a uniform gravitational field only acting in one direction[3]. OGL is a feedback guidance algorithm that depends on the difference between the current state of the vehicle and its target state as inputs. Additionally, performance is determined by two constant control gains and the estimated time to reach the target, called ”time-to-go”.

Battin demonstrates, in his text *An Introduction to the Mathematics and Methods of Astrodynamics*, the derivation of a nearly identical OGL closed-form feedback guidance solution by employing calculus of variations to solve the optimal control problem that seeks to minimize the total acceleration of a spacecraft.[2] Similar to D’Souza’s optimal control law, Battin’s derivation of OGL is optimal under the assumption of constant gravity. In the more practical case, however, where the gravitational acceleration of the spacecraft is dependent on its position, optimality is no longer guaranteed as the premise of minimizing the total acceleration of the vehicle is no longer valid. In spite of this fact, Battin’s optimal control law is still shown to be nearly optimal in a wide variety of practical applications.[2] This observation motivates the research

of OGL in applications that are more dynamically complex than planetary landing.

Guo et. al. evaluated the performance of several variations of the ZEM/ZEV feedback guidance algorithm for some classic ballistic missile intercept cases and asteroid intercept scenarios.[13] Their work demonstrated that while suboptimal, the OGL solutions were still competitive against open-loop optimal solutions.[13] Additionally OGL's feedback characteristics make it suitable to deal with uncertainties and perturbations compared to any open-loop solution. This assessment is further verified by the work of Dinius et. al. who demonstrated that the zero-effort miss / zero-effort velocity feedback guidance strategy produced near-optimal results in the case of transfer from a geostationary transfer trajectory to the L1 libration point in the Earth-Moon system using the planar restricted three-body problem as a model.[12] Although OGL was shown to be suboptimal, it succeeded in guiding the spacecraft to its target. Dinius concluded that OGL should be considered as a component of a fuel-optimal solution in the CRTBP rather than the complete solution. Guo furthered this research by augmenting the Mars descent landing scenario with targeted waypoints to facilitate the guided approach of spacecraft with thrust-limited engines. Guo et. al. additionally developed a method for calculating the optimal placement of a pre-selected number of waypoints for a descent trajectory.[26]

Ebhrami et al. joined OGL with sliding-mode control theory to derive an optimal sliding guidance law for the case of an exoatmospheric interceptor with a fixed-interval guidance time. This new guidance method has been termed optimal sliding guidance (OSG). [4, 27] This demonstrated that the easy to implement optimal guidance law derived from optimal control theory can be augmented to better handle unknown disturbances and still retain its desirability as a practical on-board guidance law. The main advantage of sliding-mode control being that the system response remains insensitive to model uncertainties and disturbances.[27] Sliding-mode control has been

used extensively in the design of missile guidance systems and in cases where the motion of a moving target can be accurately estimated or known apriori. The robustness that sliding augmentation offers, however, often comes at the cost of higher control authority requirements. It is therefore necessary to limit the control authority based on some assumed limit of perturbing forces.[27]

Wibben et. al. compared performance between OSG and OGL for Mars powered descent. This technique combines methodologies from both optimal and sliding control to create a guidance framework. With the addition of the sliding mode augmentation one can formally prove the developed OSG law is globally finite time stable to unknown, but bounded perturbations.[24] This demonstrated that the sliding guidance can provide a more robust solution in off-nominal situations, while still providing similar fuel consumption compared to regular ZEM/ZEV feedback guidance.[23, 24]

The three-body problem, which is a system comprised of three massive bodies close enough in space such that each body's motion is affected by the gravity of the other two, has been studied for centuries. Study of the three-body problem has produced approximate solutions and families of potentially useful trajectories that can only exist in a multi-body regime.[7] These discoveries have allowed mission designers to exploit the three-body dynamics in order to make missions like the International Sun-Earth Explorer (ISEE-3), the Wilkinson Microwave Anisotropy Probe (WMAP), and the James Webb Space Telescope (JWST) possible.

Study of the circular restricted three-body problem (CRTBP), a specific case of the more general three-body problem, has uncovered a host of dynamical phenomena that can be further exploited to send spacecraft further out into space at a lower fuel cost and expand our current earth and stellar observational capability. Dynamical structures of the CRTBP have revealed much about the morphology and transport of materials of the solar system, such as stable or unstable manifolds and bounding

surfaces that can be used to plan a low energy transfer trajectory across cislunar space.

Of particular interest, in recent decades, are libration point orbits. Libration points are equilibrium solutions to the CRTBP equations of motion that correspond to physical locations in space where a spacecraft can maintain a stable position relative to the other two massive bodies. Orbits about these points are periodic quasi-stable solutions. The James Webb Space Telescope is one example of a mission that will take advantage of a LPO by orbiting the Sun-Earth L2 libration point in order to maintain a static relative position to the earth.

Spacecraft operations around Earth-Moon libration points have been a topic of great interest largely due to the possibility of better facilitating lunar operations and deep space missions. The L1 and L2 libration points on either side of the moon can be potentially used as staging areas for missions to nearby planetary bodies.[25] Moreover, a spacecraft in orbit about the L2 libration point can maintain a constant line of sight with earth, thus enabling communications with any assets on the far side of the moon.[25] LPOs can also be used to supplement earth observation. As low earth orbit and geosynchronous orbit become more populated, LPOs are becoming a more attractive alternative for the positioning of satellites. A constellation of satellites around the L1 and L3 Earth-Moon libration points could achieve between 50% to 100% coverage of the earth's surface as well as continual surveillance of earth's geosynchronous region.[8]

It is well-known, however, that orbits about the colinear libration points are generally unstable. A spacecraft in an a libration point orbit must perform station-keeping in order to remain in its desired orbit. Some LPOs are more stable than others, and these orbits can be chosen for missions such that the frequency and magnitude of station-keeping maneuvers is minimized. However, this limits the mission design

space. Additionally, with the advent of low cost commercial off-the-shelf (COTS) spacecraft, there is an increasing interest in creating relatively low-budget missions to send a small spacecraft into deep space. Commanding a spacecraft with the capability of automatically performing necessary station-keeping maneuvers may be of great benefit to small teams constrained by a tight budget. Therefore, creating a guidance framework for controlling a spacecraft near the inherently unstable libration point is of current interest and motivates this investigation.

A halo orbit is a type of three-dimensional LPO that can exist in the vicinity of three libration points in a three-body system. Several halo orbit station-keeping schemes have been developed by researchers. One popular method is to establish through meticulous study of the CRTBP the most stable orbits that can satisfy missions constraints in an effort to eliminate a need for a robust control effort. Then the problem is reduced to manually commanding the spacecraft from the ground to perform regular, but less frequent, correction maneuvers. In the ISEE-3 mission, for example, station-keeping maneuvers were performed every 45 days for a halo orbit with a period of roughly 6 months.[18]

Libration point orbits and controlled flight in their vicinity is a thoroughly researched subject. Farquhar et. al. investigated the evolution of quasi-period solutions in the CRTBP in great detail, going so far as to create approximate fourth order solutions of different types of LPOs that can be used for mission planning.[9] His research has proved useful to mission planners and researchers for decades. Bando et. al. proposed a novel approach to halo orbit design and station-keeping by taking advantage of the fact that these orbits have two oscillating modes: one in the in-plane motion and one in the out-of-plane motion.[28] Their scheme seeks to employ frequency control to construct an orbit, and input-state feedback linearization to control to the reference orbit in perturbed environment.[28] Furthermore, Pavlak

and Howell developed a long-term halo orbit station-keeping strategy that constructs periodic maneuvers to position a spacecraft back onto a reference orbit based on a multiple-shooting method to satisfy end of mission constraints.[19] Furthermore they have demonstrated that their process can be optimized through direct optimization of the delta-v cost of the maneuver through direct optimization.[19] Lastly, Nazari et. al. proposed three control strategies for continuous thrust station-keeping in an Earth-Moon halo orbit based on continuous linear quadratic regulator (LQR) control and Floquet theory with periodic control gains.[20] This research showed the continuous control strategies used required less effort than continuous controllers with constant control gains.

Separately, proximity operations and orbital rendezvous in earth orbit have been studied for decades. This field is particularly prevalent in the area of manned spaceflight. Many of the Space Shuttle missions, for example, involved on-orbit docking. Spacecraft that interact with one another in this way are most conveniently described as the motion of a 'deputy' satellite moving with respect to a 'chief' satellite. This is referred to generically as spacecraft relative motion, or more specifically formation flight. Currently, a focus has been placed on future missions that will have the capability of performing impromptu proximity operations, particularly under autonomous guidance control. Sherrill et. al. proposed a method for continuous-thrust control of satellite formations in elliptical orbits by using a control law with a time-varying feedback gain derived from Lyapunov-Floquet theory.[21] The case of relative motion, in addition to the three-body problem, is an excellent candidate environment to test the performance of the OSG and OGL methods.

### 1.0.1 Problem Definition

Researchers have been broadening the application of a zero-effort error feedback guidance scheme for years and have demonstrated that its usefulness in space applications has not yet been completely explored. Therefore the purpose of this investigation is to examine how the optimal guidance law and optimal sliding guidance law perform in two complex systems that have not yet been paired with these guidance methods. The motivation for studying an autonomous guidance method for missions in low earth orbit formation flight and cis-lunar space have been established. This investigation seeks not only to derive insight into the behavior of OGL/OSG in more dynamically complex environments, but to also determine possible avenues of future research on this topic.

### 1.0.2 Outline

This paper is divided into the following segments.

Chapter 1 is an introduction to each of the topics relevant to this investigation. In this chapter, an overview of relevant literature and history of optimal sliding guidance is offered and used as motivation for research in this area. It is here that the Circular Restricted Three-Body Problem model is derived and libration point orbits are discussed. After which, the spacecraft formation flight models are developed.

Chapter 2 develops the guidance problem. It discusses and derives the methods used to construct the optimal sliding guidance method. Here there the optimal guidance law is derived, followed by a discussion of sliding-mode control theory and its application in OSG.

Chapter 3 details the methods used in this study to build the necessary components of the following simulations. This chapter discusses how the problem statement

is addressed and how exactly the results in Chapter 4 are obtained.

Chapter 4 reports on the results obtained during this investigation.

Chapter 5 concludes this report by discussing the results from Chapter 4 and provides insight into how the results influence the direction of future work in this area.

## 1.1 Circular Restricted Three-Body Problem

### 1.1.1 Equations of Motion

The derivation of the equations of motion of the three-body problem begins with describing the motion of three gravitationally attracted particles in inertial space. The position of all three masses  $m_1$ ,  $m_2$ , and  $m_3$  are located relative to their center of mass through the vectors  $\mathbf{R}_1$ ,  $\mathbf{R}_2$ , and  $\mathbf{R}_3$ , see Figure 1.1. The motion of the center of mass is defined to either be at rest or moving with a constant velocity. The center of mass is therefore adopted as an inertial origin. The three inertial acceleration equations and the gravitational potential  $U$  are then given by

$$m_i \ddot{\mathbf{R}}_i = G \sum_{j=1}^3 \frac{m_i m_j}{R_{ij}^3} \mathbf{R}_{ij} = \mathbf{F}_i \quad \text{for } i = 1, 2, 3 \quad i \neq j \quad (1.1)$$

$$U = G \sum_{1 \leq i < j \leq 3} \frac{m_i m_j}{R_{ij}} = \frac{G}{2} \sum_{i=1}^3 \sum_{j=1}^3 \frac{m_i m_j}{R_{ij}} \quad (1.2)$$

where  $G$  is the universal gravitational constant,  $\mathbf{F}_i$ , is the net resultant force acting on each mass,  $m_i$ , and  $\mathbf{R}_{ij}$  is the relative position vector defined as  $\mathbf{R}_{ij} = \mathbf{R}_j - \mathbf{R}_i$ . The potential  $U$  and the net resultant force  $\mathbf{F}_i$  are related by

$$\begin{aligned}
\mathbf{F}_1 &= \nabla_{\mathbf{R}_1} U \\
\mathbf{F}_2 &= \nabla_{\mathbf{R}_2} U \\
\mathbf{F}_3 &= \nabla_{\mathbf{R}_3} U
\end{aligned}
\tag{1.3}$$

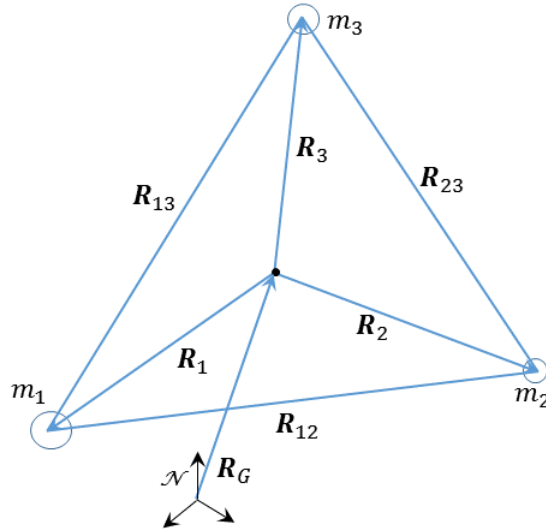


Figure 1.1: Three Body Problem in Inertial Frame

The three second-order vector differential equations given by Equation 1.1 form the basis of the three-body problem. However, the general three-body problem cannot be solved analytically. Therefore, simplifying assumptions must be made in order to further investigation. The first assumption is that the mass of the third body is much smaller than the other two bodies,  $m_3 \ll m_2 \leq m_1$ . This realistically approximates the situation of a spacecraft within the vicinity of two large planetary bodies. A spacecraft in the Sun-Earth or Earth-Moon systems are two examples of this case. Although the spacecraft is still affected by the gravity of primary bodies,  $m_1$  and  $m_2$ , due to its comparatively negligible mass the motion of  $m_1$  and  $m_2$  are independent of  $m_3$ . This motion is then characterized by the general two-body problem.[2] Thus, the

primary bodies move on conic paths with respect to their gravitational barycenter. We further simplify the problem by making the assumption that the motion of the primaries is purely circular.  $\mathbf{R}$  as the distance between the two primaries

$$\mathbf{R} = \mathbf{R}_2 - \mathbf{R}_1 \quad (1.4)$$

which is constant due to the circular orbit assumption, the angular velocity of the system can be described as

$$\omega^2 = \frac{G(m_1 + m_2)}{R^3} \quad (1.5)$$

To develop the the equations of motion of the spacecraft near the circularly orbiting primaries, it is necessary to express its inertial position vector, defined as  $\mathbf{r}$  for simplicity, in a rotating reference frame  $\mathcal{F} : \{\hat{\mathbf{e}}_r, \hat{\mathbf{e}}_\theta, \hat{\mathbf{e}}_z\}$ . The angular velocity of the rotating frame relative to some inertial frame is  $\boldsymbol{\omega} = \omega \hat{\mathbf{e}}_z$ . The position vector of the spacecraft can then described in rotating frame coordinates as

$$\mathbf{r} = r_x \hat{\mathbf{e}}_r + r_y \hat{\mathbf{e}}_\theta + r_z \hat{\mathbf{e}}_z \quad (1.6)$$

It is important to note that although the movement of the primary bodies is planar, the third mass is not similarly restricted and can move both in the orbit plane and perpendicular to it.[1] In order to find the inertial acceleration of the spacecraft by twice differentiating Equation 1.6, the transport theorem must be applied to account for the rotation of the synodic frame in the inertial derivative.[1, 10] The following is the end result, shown first in vector form and then in component form, of applying the transport theorem to the differentiation of  $\mathbf{r}$

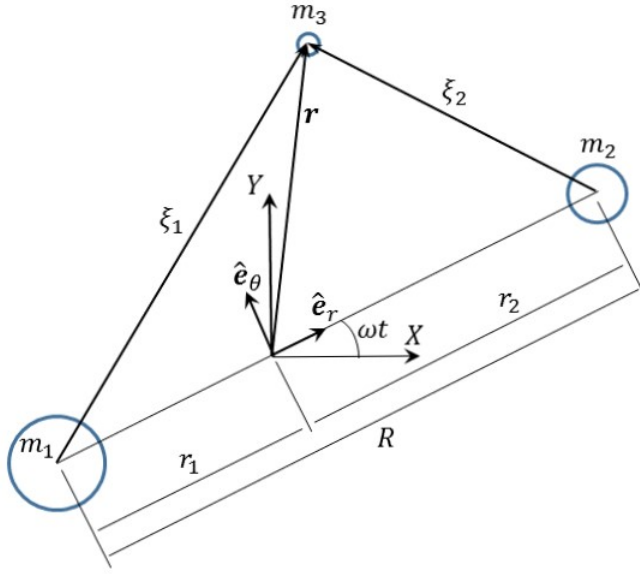


Figure 1.2: Three Body Problem Rotating Frame

$${}^{\mathcal{N}}\ddot{\mathbf{r}} = {}^{\mathcal{F}}\ddot{\mathbf{r}} + \boldsymbol{\omega} \times (\boldsymbol{\omega} \times \mathbf{r}) + 2\boldsymbol{\omega} \times \dot{\mathbf{r}} \quad (1.7)$$

$$\ddot{\mathbf{r}} = (\ddot{r}_x - 2\dot{r}_y\omega - r_x\omega^2)\mathbf{e}_r + (\ddot{r}_y + 2\dot{r}_x\omega - r_y\omega^2)\mathbf{e}_\theta + \ddot{r}_z\mathbf{e}_z \quad (1.8)$$

Taking into consideration the assumption that  $m_3$  has a negligible mass and employing the definition of the gravitational potential function in Equation 1.2, the gravitational potential on  $m_3$  is expressed as

$$U = \frac{Gm_1}{\xi_1} + \frac{Gm_2}{\xi_2} \quad (1.9)$$

where

$$\xi_i = \sqrt{(r_x - r_i)^2 + r_y^2 + r_z^2} \quad (1.10)$$

Applying Equation 1.3 to Equation 1.10 taking care to take the gradient of the po-

tential function in the rotating frame  $\mathcal{F}$  rather than the inertial frame gives the gravitational forces vectors acted upon the spacecraft by the two primary bodies.

$$\begin{aligned}
F_r &= -G \left( \frac{m_1}{\xi_1^3} (r_x - r_1) + \frac{m_2}{\xi_2^3} (r_x - r_2) \right) \\
F_\theta &= -G \left( \frac{m_1}{\xi_1^3} + \frac{m_2}{\xi_2^3} \right) r_y \\
F_z &= -G \left( \frac{m_1}{\xi_1^3} + \frac{m_2}{\xi_2^3} \right) r_z
\end{aligned} \tag{1.11}$$

Combining Equations 1.8 and 1.11 the equations of motion of the spacecraft can be written as three scalar, coupled differential equations:[1]

$$\begin{aligned}
\ddot{r}_x - 2\dot{r}_y\omega - r_x\omega^2 + G \left( \frac{m_1}{\xi_1^3} (r_x - r_1) + \frac{m_2}{\xi_2^3} (r_x - r_2) \right) &= 0 \\
\ddot{r}_y + 2\dot{r}_x\omega - r_y\omega^2 + G \left( \frac{m_1}{\xi_1^3} + \frac{m_2}{\xi_2^3} \right) r_y &= 0 \\
\ddot{r}_z + G \left( \frac{m_1}{\xi_1^3} + \frac{m_2}{\xi_2^3} \right) r_z &= 0
\end{aligned} \tag{1.12}$$

These equations of motion are more commonly expressed in their non-dimensional form. To achieve this, the non-dimensional time variable is defined as

$$\tau = \omega t = \frac{t}{T} \tag{1.13}$$

where  $T$  is the period of the system. In the case of the Earth-Moon system, this is taken to be the mean orbital period of the two bodies about their barycenter. Because the orbit is circular, the constant angular velocity  $\omega$  is equivalent to the orbital mean motion  $N$ . From Equation 1.13 it is clear that that the non-dimensional time unit  $\tau$  is equal to the angle of rotation between the synodic and inertial frames. Lastly, the

time derivative of some variable  $x$  with respect to  $\tau$  are denoted as

$$x' = \frac{dx}{d\tau} \quad (1.14)$$

Next, the measurements of position in the differential equations of motion are easily nondimensionalized by dividing them by the distance between the primary bodies,  $R$ .

$$x = \frac{r_x}{R}, \quad y = \frac{r_y}{R}, \quad z = \frac{r_z}{R}, \quad x_1 = \frac{r_1}{R}, \quad x_2 = \frac{r_2}{R} \quad (1.15)$$

Finally the mass quantities are non-dimensionalized by introducing the following parameter  $\mu$ :

$$\mu = \frac{m_2}{m_1 + m_2} \quad (1.16)$$

Typically when applying the Circular Restricted Three-Body Problem  $m_1$  and  $m_2$  are designated such that  $m_2 \leq m_1$ , so  $\mu \leq 0.5$ . From the definition of the center of mass position vector and Equation 1.16, the following relationship is made:

$$\mathbf{R}_G = \frac{m_1 \mathbf{r}_1 + m_2 \mathbf{r}_2}{m_1 + m_2} = (1 - \mu) \mathbf{r}_1 + \mu \mathbf{r}_2 = \mathbf{0} \quad (1.17)$$

Combining this with Equation 1.4 and taking into consideration that  $\mathbf{R}$ ,  $\mathbf{r}_1$ , and  $\mathbf{r}_2$  are all either parallel or anti-parallel yields the following relationships between the mass parameter and the distances of the primaries from the barycenter

$$R_1 = -\mu R \quad (1.18)$$

$$R_2 = (1 - \mu) R \quad (1.19)$$

Because each distance parameter must be normalized by the characteristic distance

between the primary bodies,  $R = 1$ . Applying this to the combination of Equations 1.15,1.18,1.19 then implies that

$$\begin{aligned}x_1 &= \mu \\x_2 &= 1 - \mu\end{aligned}\tag{1.20}$$

Furthermore,  $\omega$  is chosen such that the gravitational constant is normalized to 1 also.

$$\omega^2 R^2 = G(m_1 + m_2) = 1\tag{1.21}$$

The differential equations of motion of Equation 1.12 can now be written in non-dimensional form by combining all of these normalized equations, yielding the following three scalar differential equations of motion

$$\begin{aligned}x'' - 2y' &= x - (1 - \mu)\frac{x - x_1}{\rho_1^3} - \mu\frac{x - x_2}{\rho_2^3} \\y'' + 2x' &= \left(1 - \frac{1 - \mu}{\rho_1^3} - \frac{\mu}{\rho_2^3}\right)y \\z'' &= -\left(\frac{1 - \mu}{\rho_1^3} + \frac{\mu}{\rho_2^3}\right)z\end{aligned}\tag{1.22}$$

where the normalized relative distance  $\rho_i$  is defined as

$$\rho_i = \sqrt{(x - x_i)^2 + y^2 + z^2}\tag{1.23}$$

It is now convenient to redefine the potential function  $U$  in Equation 1.9 to include terms that account for the centripetal acceleration in the equations of motion from Equation 1.8.

$$U(r_x, r_y, r_z) = \frac{\omega^2}{2}(r_x^2 + r_y^2) + \frac{Gm_1}{\xi_1} + \frac{Gm_2}{\xi_2}\tag{1.24}$$

Again applying the normalizing equations above, the corresponding non-dimensional

potential function is found to be

$$U(x, y, z) = \frac{1}{2}(x^2 + y^2) + \frac{1 - \mu}{\rho_1} + \frac{\mu}{\rho_2} \quad (1.25)$$

The non-dimensional differential equations of motion can now be expressed more simply as

$$\begin{aligned} x'' - 2y' &= \frac{\partial U}{\partial x} \\ y'' + 2x' &= \frac{\partial U}{\partial y} \\ z'' &= \frac{\partial U}{\partial z} \end{aligned} \quad (1.26)$$

Redefining the potential function  $U$  in this way allows the equations of motion to be written in a compact form that more readily yields a perfect integral, namely the Jacobi integral. A common method of finding a constant of motion is to take the dot product of the vector equations of motion in Equation 1.26 and the velocity of  $m_3$  in the rotating frame to obtain an differential equation that can be integrated to find an expression for the constant.[14] Equation 1.26 can be expressed in compact matrix form as

$$\mathbf{r}'' + 2\tilde{\mathbf{r}}' = \frac{\partial U}{\partial \mathbf{r}} \quad (1.27)$$

where  $\tilde{\mathbf{r}}'$  is the cross-product matrix. Taking the dot product of Equation 1.27 yields

$$x''x' + y''y' + z''z' = \frac{\partial U}{\partial x}x' + \frac{\partial U}{\partial y}y' + \frac{\partial U}{\partial z}z' \quad (1.28)$$

with is easily integrated because  $U$  is a function only of position. The result if Jacobi's integral:

$$v^2 = (x'^2 + y'^2 + z'^2) = 2U - C \quad (1.29)$$

where the scalar  $C$  is determined through initial conditions. This constant is used

as a relative every measure.[1] As long as a spacecraft is not changing acceleration with thrust, at every point in the motion of the spacecraft governed by the Circular Restricted Three-Body equations the Jacobi integral must be satisfied. This also gives rise to the definition of Zero-Relative-Velocity Surfaces, which define boundaries determined by the spacecraft's kinetic energy.

### 1.1.2 Libration Points

The Circular Restricted Three Body Problem equations of motion identify five equilibrium solutions. These are stationary points that can be found by setting the relative accelerations and velocities of Equation 1.22 equal to zero. These five points are points, known as Lagrange points or libration points, all lie within the  $xy$  plane. Three points,  $L_1$ ,  $L_2$ , and  $L_3$ , are collinear along the  $x$  axis, and the remaining two,  $L_4$  and  $L_5$ , lie on either side of the  $y = 0$  plane in an equilateral triangle configuration with the primary bodies.

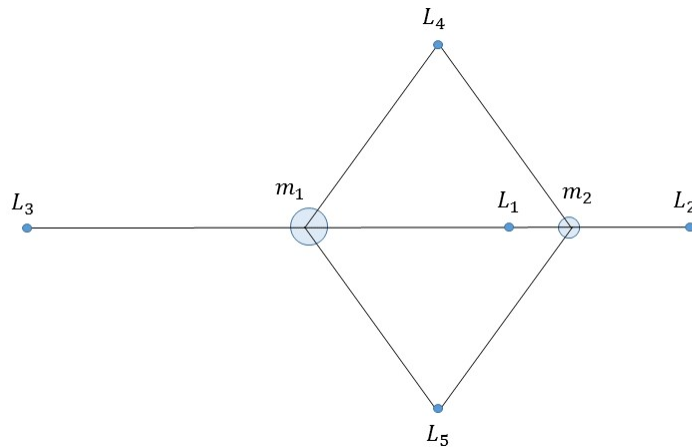


Figure 1.3: Geometric Layout of Libration Points in the  $x, y$  Plane

The positions of the collinear libration points can be easily found by substituting

zero for the values of  $y$  and  $z$  and examining the result.

$$\begin{aligned}
\left[\frac{\partial U}{\partial x}\right]_{\mathbf{r}_e} &= x_e - (1 - \mu) \frac{x_e - x_1}{\rho_{1e}^3} - \mu \frac{x_e - x_2}{\rho_{2e}^3} \\
\left[\frac{\partial U}{\partial y}\right]_{\mathbf{r}_e} &= y_e - (1 - \mu) \frac{y_e}{\rho_{1e}^3} - \mu \frac{y_e}{\rho_{2e}^3} \\
\left[\frac{\partial U}{\partial z}\right]_{\mathbf{r}_e} &= -(1 - \mu) \frac{z_e}{\rho_{1e}^3} - \mu \frac{z_e}{\rho_{2e}^3}
\end{aligned} \tag{1.30}$$

The first expression in Equation 1.30 can be used to solve for the scalar coordinate  $x_e$  for each colinear libration point.[1, 10] Substituting  $y = z = 0$  reduces the last two terms of the expression to

$$x_e - (1 - \mu) \frac{x_e - x_1}{|x_e - x_1|^3} - \mu \frac{x_e - x_2}{|x_e - x_2|^3} \tag{1.31}$$

Using the knowledge that one stationary point lies on the negative  $x$ -axis beyond  $m_1$ , one points lies in between  $m_1$  and  $m_2$ , and one point lies on the positive  $x$ -axis beyond  $m_2$ , it can be deduced that

$$(x - x_i) = \begin{cases} -|x - x_i|, & \text{if}(x - x_i) < 0 \\ |x - x_i|, & \text{if}(x - x_i) > 0 \end{cases} \tag{1.32}$$

Therefore the  $x$ -axis positions of the colinear libration points are easily found by using Equation 1.32 so apply the correct sign when canceling out terms in the denominator of Equation 1.31. This yields the following expressions for the positions of  $L_1$ ,  $L_2$ ,

and  $L_3$ :

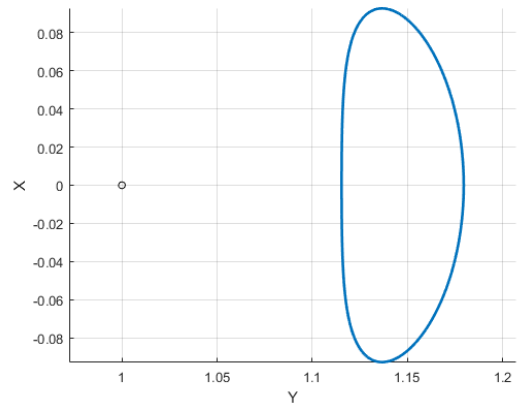
$$\begin{aligned}
 x_{L_1} &= -\frac{1-\mu}{(\mu+x)^2} + \frac{\mu}{(x-1+\mu)^2} \\
 x_{L_2} &= -\frac{1-\mu}{(\mu+x)^2} - \frac{\mu}{(x-1+\mu)^2} \\
 x_{L_3} &= \frac{1-\mu}{(\mu+x)^2} + \frac{\mu}{(x-1+\mu)^2}
 \end{aligned} \tag{1.33}$$

### 1.1.3 Libration Point Orbits

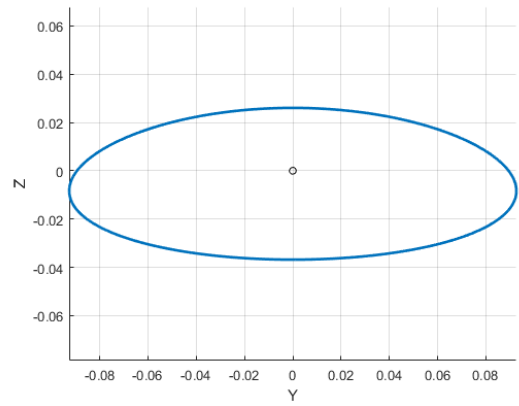
Libration point orbits (LPO) are periodic stationary orbits in the vicinity of one of the three colinear lagrange points. An infinite number of these orbits exist, however they are difficult to find since circular restricted three-body problem has no known closed-form solution. In the late 19th century, Henri Poincaré demonstrated that a possible set of solutions to the CRTBP has periodic trajectories.[7] Since then, researchers have discovered several classes of LPOs characterized by their shape, energy, and periodicity. Two orbit families have been of paramount interest in recent years: two-dimensional Lyapunov orbits, and three-dimensional halo orbits. An example halo orbit about the  $L_2$  Earth-Moon libration point is shown in Figure 1.4.

LPOs are exposed through numerical integration of the CRTBP equations of motion. Research in this area was therefore slow to advance until high-speed computers became available in the mid 20th century. Although several methods of finding LPOs have been proposed over the past fifty years, the process remains difficult unless the initial conditions for an orbit are known. Although some analytical approximations, such as the third-order Richardson Approximation, can deliver an acceptably close initial condition, linearization of the CRTBP equations of motion about the libration points can not only provide equally valid initial condition estimates, but it can also give an insight into the stability into the libration points themselves.[14]

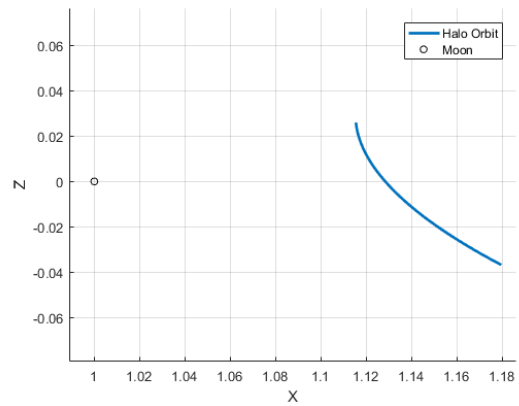
It can be shown by the linearization of the variational CRTBP equations about



(a) X-Y Plane



(b) Y-Z Plane



(c) X-Z Plane

Figure 1.4: Example Halo Orbit Near Earth-Moon L2

the points L1, L2, and L3 and subsequent analysis of each of the linearized system's eigen values that these three equilibria are saddle points with one stable mode and one unstable mode. The remaining equilibria, L4 and L5, are stable at the top of a local maximum of potential energy and hence often regarded as impractical to exploit in space missions.[14]

The linearization of the system of nonlinear dynamics about a point can be achieved by defining a variational equation to describe the 'departure' from reference trajectory and using a Taylor series expansion to approximate its derivative with respect to time.[1] For example, to linearize the system of differential equations  $\dot{\mathbf{x}} = \mathbf{f}(\mathbf{x})$  about a reference trajectory  $\mathbf{x}_r$ , the following variational equation is defined:

$$\delta\mathbf{x} = \mathbf{x} - \mathbf{x}_r \quad (1.34)$$

and its time derivative is approximated to be

$$\delta\dot{\mathbf{x}} = \dot{\mathbf{x}} - \dot{\mathbf{x}}_r \approx \frac{\partial\mathbf{f}(\mathbf{x}_r)}{\partial(\mathbf{x})}\delta\mathbf{x} \quad (1.35)$$

when higher order terms from the Taylor series expansion are ignored. Furthermore, if the reference trajectory is an equilibrium solution, as the libration points are in the circular restricted three-body problem, Equation 1.35 can be reduced to

$$\dot{\mathbf{x}} \approx \frac{\partial\mathbf{f}(\mathbf{x}_r)}{\partial(\mathbf{x})}\mathbf{x} \quad (1.36)$$

In order to apply this method to the non-dimensional equations of motion in Equation set 1.22, it is convenient to express them in their compact vector form:

$$\mathbf{r}'' + 2[\tilde{\Omega}]\mathbf{r}' + [\tilde{\Omega}]^2\mathbf{r} = -\frac{1-\mu}{\rho_1^3}(\mathbf{r} - \mathbf{r}_1) - \frac{\mu}{\rho_2^3}(\mathbf{r} - \mathbf{r}_2) = \frac{\partial U}{\partial\mathbf{r}} \quad (1.37)$$

The matrix  $[\tilde{\Omega}]$  is the skew-symmetric matrix of the non-dimensional angular velocity vector  $\Omega = [0, 0, 1]^T$ . Using this form for, the linearized variational equation is then clearly

$$\delta \mathbf{r}'' + 2[\tilde{\Omega}]\delta \mathbf{r}' + [\tilde{\Omega}]^2\delta \mathbf{r} = \frac{\partial F(\mathbf{r}_0)}{\partial \mathbf{r}}\delta \mathbf{r} \quad (1.38)$$

where  $F(\mathbf{r}_0)$  is equivalent to the vector  $\frac{\partial U}{\partial \mathbf{r}}$  evaluated on the reference point  $\mathbf{r}_0$ . By defining the state vector  $\mathbf{x}$  as

$$\mathbf{x} = [\mathbf{r}, \mathbf{r}']^T \quad (1.39)$$

Equation 1.38 can be rewritten in state space form as

$$\delta \mathbf{X}' = [\mathbf{M}(\mathbf{r}_0)]\delta \mathbf{X} \quad (1.40)$$

where

$$\mathbf{M} = \begin{bmatrix} \mathbf{0}_3 & \mathbf{I}_3 \\ \mathbf{B} & \mathbf{C} \end{bmatrix} \quad (1.41)$$

The submatrices of  $\mathbf{M}$  are then

$$\mathbf{0}_3 = 3 \times 3 \text{ zero matrix} \quad (1.42)$$

$$\mathbf{I}_3 = 3 \times 3 \text{ identity matrix} \quad (1.43)$$

$$\mathbf{B} = \begin{bmatrix} U_{xx} & U_{xy} & U_{xz} \\ U_{yx} & U_{yy} & U_{yz} \\ U_{zx} & U_{zy} & U_{zz} \end{bmatrix} \quad (1.44)$$

$$\mathbf{C} = \begin{bmatrix} 0 & 2 & 0 \\ -2 & 0 & 0 \\ 0 & 0 & 0 \end{bmatrix} \quad (1.45)$$

The eigenvalues of the matrix  $M$  indicate the local stability or instability around the chosen reference point. Therefore by setting  $\mathbf{r}_0$  equal to the vector position of a libration point, its local stability can be investigated. More notably, the state space representation also allows one to calculate a fair approximation of the initial conditions of a libration point orbit.

## 1.2 Spacecraft Formation Flight

### 1.2.1 General Equations of Relative Motion

In this section the relative orbit descriptions of two satellites for both circular and elliptic orbits are developed. It is assumed that the spacecraft are of equal type and construction, such that the relative drag on each vehicle has negligible effect on the relative orbit. The simplest type of spacecraft formation flying geometry is the leader-follower relationship shown in Figure 1.5.

In order to develop the equations of motion, one spacecraft is chosen to be a stationary point in a moving reference frame. This spacecraft is designated the "chief" satellite. Any remaining spacecraft are referred to as "deputy" satellites. The chief satellite always remains at the origin of the rotating reference frame, and a deputy satellite "orbits" this reference point. The inertial frame of reference is taken to be the Earth-Centered-Inertial (ECI) frame. The inertial chief position is given by  $\mathbf{r}_c$  and the inertial deputy position is given by  $\mathbf{r}_d$ . In order to focus on the motion of the deputy spacecraft in the rotating frame, the Hill coordinate frame is used.[1] This reference frame is also called the Local Vertical Local Horizontal (LVLH) frame.

$$\mathcal{O} : \{\hat{\mathbf{o}}_r, \hat{\mathbf{o}}_\theta, \hat{\mathbf{o}}_h\} \tag{1.46}$$

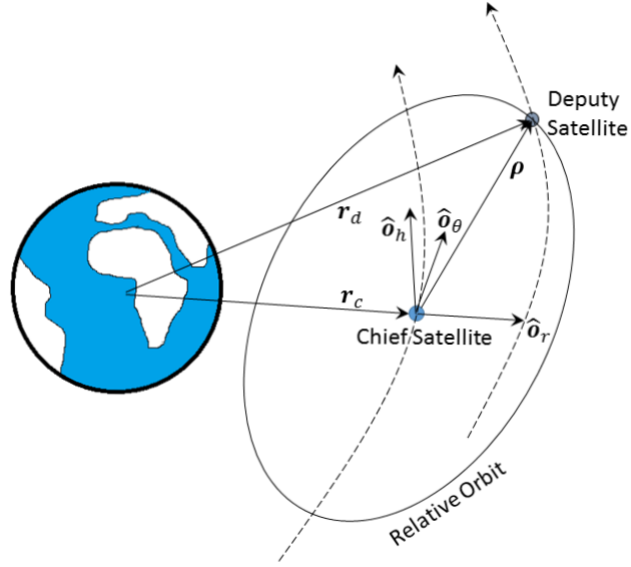


Figure 1.5: Chief-Deputy Relative Motion Illustration

The radial unit vector  $\hat{\mathbf{o}}_r$  is always parallel to the inertial vector  $\mathbf{r}_c$ . The cross-track unit vector  $\hat{\mathbf{o}}_h$  points in the direction of the chief orbit momentum vector. The down-track unit vector  $\hat{\mathbf{o}}_\theta$  completes the right handed coordinate system. The LVLH frame coordinate vectors are thus expressed as

$$\begin{aligned}
 \hat{\mathbf{o}}_r &= \frac{\mathbf{r}_c}{r_c} \\
 \hat{\mathbf{o}}_\theta &= \hat{\mathbf{o}}_h \times \hat{\mathbf{o}}_r \\
 \hat{\mathbf{o}}_h &= \frac{\mathbf{h}}{h}
 \end{aligned} \tag{1.47}$$

where  $\mathbf{h} = \mathbf{r}_c \times \dot{\mathbf{r}}_c$ . Having defined the LVLH frame, the position of a deputy spacecraft

can now be described with the vector  $\boldsymbol{\rho} = \mathbf{r}_c - \mathbf{r}_d$  as

$$\boldsymbol{\rho} = \begin{matrix} \theta \\ \left( \begin{array}{c} x \\ y \\ z \end{array} \right) \end{matrix} \quad (1.48)$$

In Equation 1.48 the vector coordinates of the position of the deputy are given in LVLH frame coordinates. In reference to the chief satellite's orbital plane, motion in the  $x, y$  plane is termed in-plane motion, while motion in the  $z$  direction is termed out-of-plane motion.

In order to derive the relative equations of motion in the LVLH frame, we first make the assumption that the satellites are both in general Keplerian orbits about a planet. The angular velocity vector of the rotating frame with respect to the ECI frame is then given by

$$\boldsymbol{\omega}_{\mathcal{O}|\mathcal{N}} = \dot{f} \hat{\mathbf{o}}_h \quad (1.49)$$

where  $f$  is the true anomaly of the chief satellite. The begin, the inertial deputy position vector is described in LVLH coordinates:

$$\mathbf{r}_d = \mathbf{r}_c + \boldsymbol{\rho} = (r_c + x) \hat{\mathbf{o}}_r + y \hat{\mathbf{o}}_\theta + z \hat{\mathbf{o}}_h \quad (1.50)$$

By twice differentiating this equation in the inertial frame through applying the Transport Theorem[1] in Equation 1.7, the deputy inertial acceleration is given as

$$\begin{aligned} \ddot{\mathbf{r}}_d = & \left( \ddot{r}_c + \ddot{x} - 2\dot{y}\dot{f} - \ddot{f}y - \dot{f}^2(r_c + x) \right) \hat{\mathbf{o}}_r \\ & + \left( \ddot{y} + 2\dot{f}(\dot{r}_c + \dot{x}) + \ddot{f}(r_c + x) - \dot{f}^2y \right) \hat{\mathbf{o}}_\theta + \ddot{z} \hat{\mathbf{o}}_h \end{aligned} \quad (1.51)$$

The inertial position vector for the chief satellite is similarly given by

$$\mathbf{r}_c = r_c \hat{\mathbf{o}}_r \quad (1.52)$$

in LVLH coordinates. Twice differentiating this expression in the inertial frame gives the inertial acceleration of the chief satellite to be

$$\ddot{\mathbf{r}}_c = \left( \ddot{r}_c - r_c \dot{f}^2 \right) \hat{\mathbf{o}}_r \quad (1.53)$$

In addition, it is assumed that both satellites obey the equations of motion of the restricted two-body problem. Applying the relative orbit description  $\ddot{\mathbf{r}} = -\frac{\mu}{r^2} \hat{\mathbf{r}}$ , where  $\mu = GM$  is the gravitational parameter, the chief acceleration is equated as

$$\ddot{\mathbf{r}}_c = \left( \ddot{r}_c - r_c \dot{f}^2 \right) \hat{\mathbf{o}}_r = -\frac{\mu}{r_c^3} \mathbf{r}_c = -\frac{\mu}{r_c^2} \hat{\mathbf{o}}_r \quad (1.54)$$

Equating the components of Equation 1.54 yields the following relationship between the chief radial acceleration

$$\ddot{r}_c = r_c \dot{f}^2 - \frac{\mu}{r_c^2} \quad (1.55)$$

The deputy acceleration expression in Equation 1.51 can be simplified by making use of the fact that orbital angular momentum,  $h$ , is a constant in Keplerian motion. The orbital angular momentum for the chief orbit is given as

$$h = r_c^2 \dot{f} \quad (1.56)$$

Since  $h$  is a constant, taking the first derivative and equating it to zero leads to the following identity

$$\dot{h} = 2r_c \dot{r}_c \dot{f} + r_c^2 \ddot{f} = 0 \quad (1.57)$$

which is used to solve for the true anomaly acceleration. Thus,  $\ddot{f}$  is found to be

$$\ddot{f} = -2\frac{\dot{r}_c}{r_c}\dot{f} \quad (1.58)$$

Lastly, utilizing the Keplerian orbital motion identity relates the semi-latus rectum,  $p$ , to the orbit angular momentum,  $p = \frac{h^2}{\mu}$ , Equation 1.55 can be rewritten as

$$\ddot{r}_c = r_c \dot{f}^2 \left(1 - \frac{r_c}{p}\right) \quad (1.59)$$

By Equations 1.58 and 1.59 in for the terms  $\ddot{r}_c$  and  $\ddot{f}$  in Equation 1.51, the deputy inertial acceleration is now given as

$$\begin{aligned} \ddot{\mathbf{r}}_d = & \left( \ddot{x} - 2\dot{f} \left( \dot{y} - y\frac{\dot{r}_c}{r_c} \right) - x\dot{f}^2 - \frac{\mu}{r_c^2} \right) \hat{\mathbf{o}}_r \\ & + \left( \ddot{y} + 2\dot{f} \left( \dot{x} - x\frac{\dot{r}_c}{r_c} \right) - y\dot{f}^2 \right) \hat{\mathbf{o}}_\theta + \ddot{z}\hat{\mathbf{o}}_h \end{aligned} \quad (1.60)$$

The deputy satellite is also under the influence of restricted two-body motion. Therefore the relative restricted two-body orbit equation is used to describe its motion as

$$\ddot{\mathbf{r}}_d = -\frac{\mu}{r_d^3}\mathbf{r}_d + \mathbf{u} \quad (1.61)$$

where  $\mathbf{u}$  is a control input in the form of an acceleration, and magnitude  $r_d$  is given as the norm of the vector  $\mathbf{r}_d$ :

$$r_d = \sqrt{(r_c + x)^2 + y^2 + z^2} \quad (1.62)$$

Finally, equating Equations 1.60 and 1.61 yields the following exact nonlinear differ-

ential equations of relative motion.

$$\ddot{x} - 2\dot{f} \left( \dot{y} - y \frac{\dot{r}_c}{r_c} \right) - x f^2 - \frac{\mu}{r_c^2} = -\frac{\mu}{r_d^3} (r_c + x) + u_x \quad (1.63)$$

$$\ddot{y} + 2\dot{f} \left( \dot{x} - x \frac{\dot{r}_c}{r_c} \right) - y f^2 = -\frac{\mu}{r_d^3} y + u_y \quad (1.64)$$

$$\ddot{z} = -\frac{\mu}{r_d^3} z + u_z \quad (1.65)$$

These equations of motion are valid for both circular and eccentric orbits. However, they are not valid for perturbed orbital motion as that would nullify the Keplerian orbit assumptions made in the derivation.

### 1.2.2 Linearized Relative Equations of Motion and the Clohessy-Wiltshire-Hill Equations

The exact nonlinear relative equations of motion can be simplified if the deputy and chief satellite orbit radii are very close. That is, simplifying assumptions can be made if the relative orbit coordinates  $(x, y, z)$  are small compared to the chief orbit radius.[1] From Equation 1.62, the first term in the square root can be expanded out in order to group all quadratic terms in the expression together. If the simplifying assumption of similar deputy and chief orbit radii can be made, then the quadratic terms can be ignored. This is shown in the following expression for  $r_d$ :

$$r_d = r_c \sqrt{1 + 2\frac{x}{r_c} + \frac{x^2 + y^2 + z^2}{r_c^2}} \approx r_c \sqrt{1 + 2\frac{x}{r_c}} \quad (1.66)$$

The set of kinematic differential equations given in Equations 1.63 through 1.65 can be expressed in the following compact form

$$\ddot{\mathbf{r}}_d = -\frac{\mu}{r_d^3} \mathbf{r}_d \quad (1.67)$$

Substituting Equation 1.66 into the expression  $-\frac{\mu}{r_d^3}$  from Equation 1.67 and applying the binomial approximation  $(1+x)^\alpha \approx 1 + \alpha x$  to the result yields the the following approximation:[1]

$$\frac{\mu}{r_d^3} \approx \frac{\mu}{r_c^3} \left(1 - 3\frac{x}{r_c}\right) \quad (1.68)$$

To continue the linearization of the equations of motion, it is convenient to eradicate the cubic term in coefficient  $\frac{\mu}{r_d^3}$ . This is accomplished by again using the semi-latus rectum and angular momentum identities  $p = \frac{h^2}{\mu}$  and  $h = r_c^2 \dot{f}$  to express the coefficient in the following form:

$$\frac{\mu}{r_c^3} = \frac{r_c}{p} \dot{f}^2 \quad (1.69)$$

Any explicit dependence on  $r_d$  is eliminated from the equations of relative motion by inserting the results from Equations 1.68 and 1.69 into the right-hand side of Equation 1.55. The right-hand side of the equation is then approximated to be

$$-\frac{\mu}{r_d^3} \begin{pmatrix} r_c + x \\ y \\ z \end{pmatrix} \approx -\frac{\mu}{r_c^3} \left(1 - 3\frac{x}{r_c}\right) \begin{pmatrix} r_c + x \\ y \\ z \end{pmatrix} \approx -\frac{r_c}{p} \dot{f}^2 \begin{pmatrix} r_c - 2x \\ y \\ z \end{pmatrix} \quad (1.70)$$

Finally, the Linearized Equations of Relative Motion (LERM) are derived by substituting the vector Equation 1.70 into scalar Equations 1.63 through 1.65 component-

wise. The result yields the following simplified equations of motion:

$$\begin{aligned}
\ddot{x} - x f^2 \left(1 + 2\frac{r_c}{p}\right) - 2\dot{f} \left(\dot{y} - y\frac{\dot{r}_c}{r_c}\right) &= u_x \\
\ddot{y} + 2\dot{f} \left(\dot{x} - x\frac{\dot{r}_c}{r_c}\right) y f^2 \left(1 - \frac{r_c}{p}\right) &= u_y \\
\ddot{z} + \frac{r_c}{p} f^2 z &= u_z
\end{aligned} \tag{1.71}$$

Furthermore, if both orbits of the chief and deputy spacecraft are assumed to be circular, then  $p = r_c$ ,  $\dot{r}_c = 0$ , and the orbital mean motion  $n$ , is equal to  $\dot{f}$ . The linearized equations can then be further simplified into the following reduced form, known as the Clohessy-Wiltshire-Hill (CWH) equations:

$$\begin{aligned}
\ddot{x} - 2n\dot{y} - 3n^2x &= u_x \\
\ddot{y} + 2n\dot{x} &= u_y \\
\ddot{z} + n^2z &= u_z
\end{aligned} \tag{1.72}$$

Both the LERM and CWH equations of motion are simple to integrate numerically inside the control loop of the ZEM/ZEV guidance algorithm. The incremental steps in simplification between the exact equations of relative motion, the linearized equations, and the CWH equations provide a basis for incrementally increasing the complexity of the model dynamics in the test environment for the controller.

# Guidance Problem Development

## 2.1 Zero-Effort Miss/Zero-Effort Velocity

In formulating the spacecraft guidance problem for use in the Circular Restricted Three-Body Problem and in relative motion case of the Restricted Two-Body Problem, the spacecraft dynamics in both cases is modeled using a simple dynamical model. By combining the equations of motion derived in the previous chapter into one term,  $\mathbf{g}(\mathbf{r}, t)$ , the equations of motion of the spacecraft can be synthetically given in the following set of vector differential equations.

$$\begin{aligned}\dot{\mathbf{r}} &= \mathbf{v} \\ \dot{\mathbf{v}} &= \mathbf{g}(\mathbf{r}, t) + \mathbf{a}_C(t)\end{aligned}\tag{2.1}$$

where

$$\mathbf{r} = [x, y, z]^T \quad \mathbf{v} = [v_x, v_y, v_z]^T\tag{2.2}$$

In this formulation, the vector  $\mathbf{g}(\mathbf{r}, t)$  represents all external forces acting on the spacecraft. The last term in total acceleration expression,  $\dot{\mathbf{v}}$ , of Equation 2.1, here depicted by  $\mathbf{a}_c$  though more commonly depicted as  $\mathbf{u}$  in most control problem formulations, is the commanded acceleration that drives the spacecraft to a desired state.

The position and velocity of the vehicle at a specified final time,  $t_f$ , can be formally determined using the knowledge of the spacecraft's state at an interim time  $t$  and by integrating the expressions in Equation 2.1. Performing this integration we obtain the following

$$\mathbf{v}(t_f) = \mathbf{v}(t) + \int_t^{t_f} (\mathbf{g}(\mathbf{r}, \tau) + \mathbf{a}_C(t)) d\tau \quad (2.3)$$

$$\mathbf{r}(t_f) = \mathbf{r}(t) + \mathbf{v}(t)t_{go} + \int_t^{t_f} \int_{\tau'}^{t_f} (\mathbf{g}(\mathbf{r}, \tau') + \mathbf{a}_C(\tau')) d\tau' d\tau \quad (2.4)$$

The term  $t_{go}$  in Equation 2.4 is termed "time to-go". It is the time required to reach the desired target position and velocity.[3]

Next, we introduce the zero-effort error definitions. Ebrahimi et al. introduced the concept of zero-effort velocity in addition to the well known zero-effort miss distance to be utilized in the optimal sliding-mode control problem.[4] The zero-effort miss error, **ZEM**, is the distance that the interceptor vehicle will miss its target if it makes no corrective maneuvers after time  $t$ . The zero-effort velocity, **ZEV** error is similarly defined only with respect to the vehicle's velocity.

$$\mathbf{ZEM}(t) = \mathbf{r}_f - \mathbf{r}(t_f), \quad \mathbf{a}_C(\tau) = \mathbf{0}, \quad \tau \in (t, t_f] \quad (2.5)$$

$$\mathbf{ZEV}(t) = \mathbf{v}_f - \mathbf{v}(t_f), \quad \mathbf{a}_C(\tau) = \mathbf{0}, \quad \tau \in (t, t_f] \quad (2.6)$$

Both expressions for zero-effort miss and zero-effort velocity can be expressed as functions of the spacecraft's current position, velocity, and time-to-go by substituting Equations 2.3 and 2.4 into Equations 2.5 and 2.6.

$$\mathbf{ZEV}(t) = \mathbf{v}_f - \mathbf{v}(t) - \int_t^{t_f} \mathbf{g} d\tau \quad (2.7)$$

$$\mathbf{ZEM}(t) = \mathbf{r}_f - \mathbf{r}(t) - \mathbf{v}(t)t_{go} - \int_t^{t_f} \int_t^{t_f} \mathbf{g} d\tau' d\tau \quad (2.8)$$

Each of the zero-effort error terms can be computed on-line by the numerical integration of the unperturbed equations of motion. Thus, it is beneficial to construct a control law that explicitly depends on  $\mathbf{ZEM}$ ,  $\mathbf{ZEV}$ , and  $t_{go}$ .

## 2.2 Optimal Guidance Law

One of the key elements in optimal sliding guidance is the ability to obtain analytically a closed loop guidance law that minimizes the overall control effort. Most optimal control problems cannot be solved analytically due to the fact that the necessary conditions for optimality are generally nonlinear, hard-to-solve, second-order differential equations with split boundary conditions. However, it can be demonstrated that an analytical closed-form solution is possible under certain simplifying conditions for the case of guided planetary landing.[3, 2] In order to derive what is termed the optimal guidance law (OGL),[23, 24, 4, 13] we must make the assumption that the  $\mathbf{g}$  is a constant vector.

The methodology employed to determine the optimal guidance law as a function of the zero-effort errors is similar to the analysis presented by D'Souza[3], who derived the optimal acceleration command for a powered landing as a function of position error, velocity error, and time-to-go. This analysis was furthered by Guo et. al.[26, 13, 15] whose methodology to formulate the control law is used here. Both guidance algorithms are simple to implement which encourages their attraction as a guidance approach.

To begin, the optimal control problem is formulated as follows:

$$\text{minimize } J(\mathbf{a}_C) = \frac{1}{2} \int_t^{t_f} \mathbf{a}_C(\tau)^T \mathbf{a}_C(\tau) d\tau \quad (2.9)$$

Subject to

$$\begin{cases} \dot{\mathbf{r}} &= \mathbf{v} \\ \dot{\mathbf{v}} &= \mathbf{g}(t) + \mathbf{a}_C(t) \end{cases} \quad (2.10)$$

With the following boundary conditions

$$\begin{cases} \mathbf{r}(t) &= \mathbf{r} \\ \mathbf{r}(t_f) &= \mathbf{r}_f \\ \mathbf{v}(t) &= \mathbf{v} \\ \mathbf{v}(t_f) &= \mathbf{v}_f \end{cases} \quad (2.11)$$

For the purposes of the derivation it is also assumed that the commanded acceleration, i.e. thrust, is unbounded. Applying variational methods to the general optimal control problem formulation, one can establish the necessary conditions for optimality.[6] (optimal control theory) Consider the following general optimal control problem:

$$\text{minimize } J(\mathbf{u}) = h(\mathbf{x}(t_f), t_f) + \int_{t_0}^{t_f} g(\mathbf{x}(t), \mathbf{u}(t), t) dt \quad (2.12)$$

subject to the following vector differential state equation

$$\dot{\mathbf{x}}(t) = \mathbf{a}(\mathbf{x}(t), \mathbf{u}(t), t) \quad (2.13)$$

where  $\mathbf{u}(t)$  is a vector of control input. Note, Equation 2.1 can easily be expressed in

this compact manner, where  $\dot{\mathbf{x}} = [\dot{\mathbf{r}}, \dot{\mathbf{v}}]^T$ . The fundamental theorem of the calculus of variations states that if the trajectory  $\mathbf{x}^*$  is an extremal, the variation of the functional  $J$  must vanish on  $\mathbf{x}^*$ , that is

$$\delta J(\mathbf{x}^*, \delta \mathbf{x}) = 0 \quad (2.14)$$

Note, the asterisk here denotes an optimal case. Applying this condition to the cost functional in Equation 2.12 and using variational methods the following necessary conditions can be derived.[6] These conditions can be conveniently expressed as partial derivatives of the Hamiltonian function  $\mathcal{H}$ .

$$\mathcal{H}(\mathbf{x}(t), \mathbf{u}(t), \mathbf{p}(t), t) = g(\mathbf{x}(t), \mathbf{u}(t), t) + \mathbf{p}^T(t)[\mathbf{a}(\mathbf{x}(t), \mathbf{u}(t), t)] \quad (2.15)$$

The necessary conditions are

$$\dot{\mathbf{x}}^*(t) = \frac{\partial \mathcal{H}}{\partial \mathbf{p}}(\mathbf{x}^*(t), \mathbf{u}^*(t), \mathbf{p}^*(t)) \quad (2.16)$$

$$\dot{\mathbf{p}}^*(t) = -\frac{\partial \mathcal{H}}{\partial \mathbf{x}}(\mathbf{x}^*(t), \mathbf{u}^*(t), \mathbf{p}^*(t), t) \quad (2.17)$$

$$\mathbf{0} = \frac{\partial \mathcal{H}}{\partial \mathbf{u}}(\mathbf{x}^*(t), \mathbf{u}^*(t), \mathbf{p}^*(t), t) \quad (2.18)$$

with the transversality condition

$$\begin{aligned} & \left[ \mathcal{H}(\mathbf{x}^*(t_f), \mathbf{u}^*(t_f), \mathbf{p}^*(t_f)) + \frac{\partial h}{\partial t}(\mathbf{x}^*(t_f), t_f) \right] \delta t_f + \\ & \left[ \frac{\partial h}{\partial \mathbf{x}}(\mathbf{x}^*(t_f), t_f) - \mathbf{p}^*(t_f) \right]^T \delta \mathbf{x}_f = 0 \end{aligned} \quad (2.19)$$

The variable  $\mathbf{p}$  is the vector of lagrange multipliers, also known as costates,  $\mathbf{p} = [p_1, p_2, \dots, p_n]^T$  where  $n$  is the dimension of the state vector  $\mathbf{x}$ .

An optimal control law can be analytically derived from inserting the the optimal

control problem formulated from Equations 2.9 to 2.11 into the necessary condition Equations 2.16 - 2.19. Using the standard form of the cost functional, the definition of the control Hamiltonian, and the cost functional in Equation 2.12, the Hamiltonian function is written as

$$\mathcal{H} = \frac{1}{2} \mathbf{a}_C^T \mathbf{a}_C + \mathbf{p}_r^T \mathbf{v} + \mathbf{p}_v^T (\mathbf{g} + \mathbf{a}_C) \quad (2.20)$$

where  $\mathbf{p}_r$  and  $\mathbf{p}_v$  are the costate vectors associated with position and velocity vectors, respectively. Due to the simplification that  $\mathbf{g}$  is a constant vector, the costate equations and optimality condition given in Equations 2.17 and 2.18 are given as

$$\dot{\mathbf{p}}_r = -\frac{\partial \mathcal{H}}{\partial \mathbf{r}} = 0 \quad (2.21)$$

$$\dot{\mathbf{p}}_v = -\frac{\partial \mathcal{H}}{\partial \mathbf{v}} = -\mathbf{p}_r \quad (2.22)$$

$$\frac{\partial \mathcal{H}}{\partial \mathbf{a}_c} = 0 \rightarrow \mathbf{a}_c = -\mathbf{p}_v \quad (2.23)$$

Integrating Equations 2.21 and 2.22 and using the definition of time-t-go,  $t_{go} = t_f - t$  the following solutions are obtained:

$$\mathbf{p}_r = \mathbf{p}_r(t_f) \quad (2.24)$$

$$\mathbf{p}_v = t_{go} \mathbf{p}_r(t_f) + \mathbf{p}_v(t_f) \quad (2.25)$$

The optimal control solution can then be expressed as

$$\mathbf{a}_C = -t_{go} \mathbf{p}_r(t_f) - \mathbf{p}_v(t_f) \quad (2.26)$$

The position and velocity can then be rewritten in terms of the costates by integrating

Equation 2.10.

$$\mathbf{v}(t) = \frac{t_{go}^2}{2} \mathbf{p}_r(t_f) + t_{go} \mathbf{p}_v(t_f) - \int_t^{t_f} \mathbf{g}(\tau) d\tau + \mathbf{v}(t_f) \quad (2.27)$$

$$\mathbf{r}(t) = -\frac{t_{go}^3}{6} \mathbf{p}_r(t_f) - \frac{t_{go}^2}{2} \mathbf{p}_v(t_f) + \int_t^{t_f} \int_t^{t_f} \mathbf{g}(\tau') d\tau' d\tau - t_{go} \mathbf{v}(t_f) + \mathbf{r}(t_f) \quad (2.28)$$

Combining Equations 2.27 and 2.28 gives

$$\mathbf{p}_r(t_f) = \frac{6(v + v_f)}{t_{go}^2} + \frac{12(r - r_f)}{t_{go}^3} - \frac{12 \int_t^{t_f} \int_t^{t_f} \mathbf{g}(\tau') d\tau' d\tau}{t_{go}^3} + \frac{6 \int_t^{t_f} \mathbf{g}(\tau) d\tau}{t_{go}^2} \quad (2.29)$$

$$\mathbf{p}_v(t_f) = -\frac{2(v + 2v_f)}{t_{go}} - \frac{6(r - r_f)}{t_{go}^2} + \frac{6 \int_t^{t_f} \int_t^{t_f} \mathbf{g}(\tau') d\tau' d\tau}{t_{go}^2} - \frac{2 \int_t^{t_f} \mathbf{g} d\tau}{t_{go}} \quad (2.30)$$

By inserting these equations into Equation 2.26 we obtain

$$\mathbf{a}_c = \frac{6(r - r_f)}{t_{go}^2} - \frac{2(v_f + 2v)}{t_{go}} + \frac{6 \int_t^{t_f} \int_t^{t_f} \mathbf{g}(\tau') d\tau' d\tau}{t_{go}^2} - \frac{4 \int_t^{t_f} \mathbf{g} d\tau}{t_{go}} \quad (2.31)$$

Splitting the second term of this equation into

$$\frac{2(v_f - v)}{t_{go}} + \frac{6vt_{go}}{t_{go}^2} \quad (2.32)$$

allowing the acceleration command law to be rewritten as

$$\mathbf{a}_c = \frac{6(r_f - (\mathbf{r} + t_{go}\mathbf{v}))}{t_{go}^2} - \frac{2(v_f - v)}{t_{go}} + \frac{6 \int_t^{t_f} \int_t^{t_f} \mathbf{g}(\tau') d\tau' d\tau}{t_{go}^2} - \frac{4 \int_t^{t_f} \mathbf{g} d\tau}{t_{go}} \quad (2.33)$$

Utilizing the definitions of zero-effort miss and zero-effort velocity in Equations 2.7 and 2.8, the command law can be written in a more compact form as

$$\mathbf{a}_c = \frac{6}{t_{go}^2} \mathbf{ZEM}(t) - \frac{2}{t_{go}} \mathbf{ZEV}(t) \quad (2.34)$$

It is important to note that a closed-loop analytical solution is not possible if  $\mathbf{g}$  is nonuniform, as it is in the case of  $\mathbf{g} = f(\mathbf{r}, t)$ . The constants 6 and  $-2$  are from this point on referred to as  $k_R$  and  $k_V$  respectively.

## 2.3 Sliding Guidance Development

Wibben et. al. first combined the following controller with ZEM/ZEV feedback guidance (OGL) to create control law termed Optimal Sliding Guidance (OSG). This was done in an effort to make the former more robust against bounded but unknown perturbations. It has been shown that the addition of a term, defined by a sliding surface, in the optimal feedback control law can create a more robust and accurate guidance algorithm than OGL in the case of a perturbed power descent phase of planetary landing.[23] Wibben et. al. also formally proved that the following optimal sliding guidance law is globally finite-time stable.

### 2.3.1 Sliding Mode Control Theory

Designing control laws that achieve a desired performance and stability in a closed-loop system in the presence of uncertainties or unknown perturbing forces is a formidable task. The sliding-mode control technique is one methodology of creating such a robust control algorithm. Sliding control is based on the observation that it is much easier to control non-linear first order systems than than it is to control  $n$ -th order systems (where  $n \geq 2$ ).[22] This method of control dictates that if a system of  $n$ -th order differential equations can be transformed into a system of first order state space equations, more robust control can be achieved. Though this is generally done at the incurred cost of higher control activity.

Consider the following single-input  $n$ th order dynamical system:

$$\frac{d^n}{dt^n} \mathbf{x} = f(\mathbf{x}) + b(\mathbf{x})u \quad (2.35)$$

Here,  $x$  is a scalar output,  $u$  is the control input, and  $\mathbf{x}$  is the state vector of the system. The system dynamics given as  $f(\mathbf{x})$  and the control gain  $b(\mathbf{x})$  are unknowns, however it is assumed that each has a known upper bound. It is desired to create a controller that will force the state  $\mathbf{x}$  to track to a desired target  $\mathbf{x}_d$  in the presence of model uncertainties. In order to achieve this, a time-varying surface is introduced as a function of the tracking error  $\tilde{\mathbf{x}} = \mathbf{x} - \mathbf{x}_d$  by the following scalar equation:

$$\mathbf{s}(\mathbf{x}, t) = \left( \frac{d}{dt} + \lambda \right)^{n-1} \tilde{\mathbf{x}} = 0 \quad (2.36)$$

For the case of  $n = 2$ , for example, the surface,  $\mathbf{s}$ , would be given as

$$\mathbf{s}(\mathbf{x}, t) = \dot{\tilde{\mathbf{x}}} + \lambda \tilde{\mathbf{x}} = 0 \quad (2.37)$$

where the parameter  $\lambda$  is always a positive scalar ( $\lambda > 0$ ). [25] With the definition the surface  $\mathbf{s}(\mathbf{x}, t)$ , the tracking problem is reduced to the problem of driving the surface to zero. That is, in order to drive the state error variables to zero, the variable  $\mathbf{s}$ , due to the way it is defined, must also be driven to zero by the means of a control input  $u$ . Thus, the problem is now a first order stabilization problem.

In order to ensure system stability, the following candidate Lyapunov function is selected:

$$V(\mathbf{s}) = \frac{1}{2} \mathbf{s}^T \mathbf{s} = \frac{\|\mathbf{s}\|^2}{2} \quad (2.38)$$

By the definition of a Lyapunov function, the following conditions must hold true for

the system  $\dot{\mathbf{s}} = f(\mathbf{s})$  to be asymptotically stable

$$\begin{aligned} V(0) &= 0 \\ V(\mathbf{s}) &> 0 & \mathbf{s} \neq \mathbf{0} \\ \dot{V}(\mathbf{s}) &= \mathbf{s}^T \dot{\mathbf{s}} \leq 0 & \mathbf{s} \neq \mathbf{0} \end{aligned} \tag{2.39}$$

From the definition of the candidate Lyapunov function, the following expression is created that ensures that all three stability criteria are satisfied over the state space domain:

$$\frac{1}{2} \frac{d}{dt} \mathbf{s}^2 \leq -\eta |s| \tag{2.40}$$

where  $\eta$  is a strictly positive constant. All system trajectories will converge on the surface  $\mathbf{s}$ , if a control law is chosen such that Equation 2.40 is always satisfied.[23] Equation 2.40 is known as the "sliding constraint" because system trajectories converge on the "sliding" surface and then slide along it to the origin.

The control law is generally obtained by substituting the definition of the sliding surface, Equation 2.37, and the system dynamics, Equation 2.35, into the expression for the sliding condition, Equation 2.40. Assuming the control gain  $b(\mathbf{x}) = 1$  and performing the aforementioned calculation, the control law is found to be:[23]

$$u = -f(\mathbf{x}) + \ddot{\mathbf{x}}d - \lambda \dot{\tilde{\mathbf{x}}} \tag{2.41}$$

However, since this control law explicitly depends on  $f(\mathbf{x})$ , it necessitates that the plant dynamics be known ahead of time which violates our previous assumptions. Therefore, the control law must be adjusted to account for unknown system dynamics by adding a discontinuous term across the surface  $\mathbf{s} = 0$  is added. This new control

law is given as

$$u = \hat{u} - \Phi \text{sign}(\mathbf{s}) \quad (2.42)$$

where  $\hat{u}$  is an approximation of the original control law in Equation 2.41:

$$\hat{u} = -\hat{f}(\mathbf{x}) + \ddot{\mathbf{x}}d - \lambda\dot{\mathbf{x}} \quad (2.43)$$

Thus, choosing a value of  $\Phi > 0$  that is sufficiently large guarantees that the sliding condition is satisfied.

### 2.3.2 Design of Optimal Sliding Guidance (OSG)

The Optimal Guidance Law derived in section 2.2 can be augmented with a nonlinear sliding control mode as was done to the example control law in section 2.3.1 in order to provide a more robust guidance algorithm. To implement this approach, we begin by modifying the OGL control law given by Equation 2.34 to take the form of the sliding mode augmented control law given by Equation 2.42. This is done by simply appending what is known as the sliding term to the ZEM/ZEV feedback control law:

$$\mathbf{a}_C(t) = \frac{k_R}{t_{go}^2} \mathbf{ZEM}(t) + \frac{k_V}{t_{go}} \mathbf{ZEV}(t) - \Phi \text{sign}(\mathbf{s}) \quad (2.44)$$

The tracking error  $\tilde{\mathbf{x}}$  defined in the sliding control problem of the previous section is in essence the same quantity as the ZEM term from the OGL formulation. Similarly, the tracking error's first order time derivative is in essence the same quantity as ZEV. Therefore, the sliding surface for this control law is defined as

$$\mathbf{s} = \mathbf{ZEV} + \lambda \mathbf{ZEM} = 0 \quad (2.45)$$

which matches the form of Equation 2.37. It is clear from this definition that the sliding surface approaches zero as the terms ZEM and ZEV both approach zero.

The guidance law must be able to drive all system trajectories to the sliding surface. Therefore in order to study the stability using a Lyapunov function, it is first necessary to examine the dynamics of the sliding surface. Taking the derivative of the sliding surface gives

$$\dot{\mathbf{s}} = \mathbf{Z}\dot{\mathbf{E}}\mathbf{V} + \lambda\mathbf{Z}\dot{\mathbf{E}}\mathbf{M} + \dot{\lambda}\mathbf{Z}\mathbf{E}\mathbf{M} \quad (2.46)$$

Differentiating Equations 2.7 and 2.8 with respect to time yields

$$\mathbf{Z}\dot{\mathbf{E}}\mathbf{V} = \frac{d}{dt} \left( \mathbf{v}_f - \mathbf{v}(t) - \int_t^{t_f} \mathbf{g} d\tau \right) = \dot{\mathbf{v}}(t) + \mathbf{g} = -\mathbf{a}_c \quad (2.47)$$

$$\mathbf{Z}\dot{\mathbf{E}}\mathbf{M} = \mathbf{r}_f - \mathbf{r}(t) - \mathbf{v}(t)t_{go} - \int_t^{t_f} \int_t^{t_f} \mathbf{g} d\tau' d\tau = -\dot{\mathbf{v}}(t)t_{go} + \mathbf{g}t_{go} = -\mathbf{a}_c t_{go} \quad (2.48)$$

Substituting the zero-effort error derivatives into Equation 2.46 simplifies the sliding surface derivative to

$$\dot{\mathbf{s}} = (1 + \lambda t_{go})\mathbf{a}_c + \dot{\lambda}\mathbf{Z}\mathbf{E}\mathbf{M} \quad (2.49)$$

The OGL control law can then be substituted into the derivative to produce

$$\dot{\mathbf{s}} = -(1 + \lambda t_{go}) \left( \frac{k_R}{t_{go}^2} \mathbf{Z}\mathbf{E}\mathbf{M} + \frac{k_V}{t_{go}} \mathbf{Z}\mathbf{E}\mathbf{V} \right) + \dot{\lambda}\mathbf{Z}\mathbf{E}\mathbf{M} \quad (2.50)$$

In an effort to express  $\dot{\mathbf{s}}$  as a function of  $\mathbf{s}$ , the following relations between the remain-

ing parameters  $\lambda$ ,  $k_R$ ,  $k_V$ , and  $t_{go}$  are created:

$$K(t) = (1 + \lambda t_{go}) \frac{k_V}{t_{go}} \quad (2.51)$$

$$\lambda K(t) = (1 + \lambda t_{go}) \frac{k_R}{t_{go}^2} - \dot{\lambda} \quad (2.52)$$

$$\lambda = \frac{k_R}{k_V t_{go}} \quad (2.53)$$

Equation 5.20 can now be simplified to be

$$\dot{\mathbf{s}} = -K(t)\mathbf{s} \quad (2.54)$$

This demonstrates that the sliding surface behaves as a non-linear first order system, and that its dynamics depend explicitly on the parameters time-to-go. Inserting the sliding term into the OGL control law and deriving  $\dot{\mathbf{s}}$  gives

$$\dot{\mathbf{s}} = -K(t)\mathbf{s} - \Phi' \text{sign}(s) \quad (2.55)$$

where  $\Phi'$  is some scalar multiple of  $\Phi$ . By defining the candidate Lyapunov function as  $V(\mathbf{s}) = \frac{1}{2}\mathbf{s}^T\mathbf{s}$ , the first two conditions for asymptotic stability in Equation set 2.39 are satisfied. Substituting Equation 2.53 into Equation 2.51 and utilizing the optimal values for  $k_R$  and  $k_V$  from the derivation of the OGL control law, Equation 2.54 is rewritten as

$$\dot{\mathbf{s}} = -\frac{4}{t_{go}}\mathbf{s} \quad (2.56)$$

The candidate Lyapunov function is shown by the following progression to be contin-

uously differentiable and positive definite on the set  $\{\mathbf{s} \in \mathbb{R}^n | \mathbf{s} \neq \mathbf{0}\}$

$$\dot{V} = \mathbf{s}^T \dot{\mathbf{s}} \quad (2.57)$$

$$= \mathbf{s}^T \left( -\frac{4}{t_{go}} \mathbf{s} - \Phi' \text{sign}(\mathbf{s}) \right) \quad (2.58)$$

$$= -\frac{4}{t_{go}} \mathbf{s}^T \mathbf{s} - \Phi' |s| \quad (2.59)$$

$$= -\frac{4}{t_{go}} \|\mathbf{s}\|^2 - \Phi' |s| \leq 0 \quad (2.60)$$

As long as the restriction  $\Phi' > 0$ , the system is globally asymptotically stable about the origin. Furthermore, Wibben et. al. has proven that this implementation of optimal sliding guidance is globally finite-time stable.[23]

# Methods

The performance of both OGL and OSG algorithms are evaluated by first implementing guidance schemes in the models established in sections 1.1 and 1.2. Expended fuel mass, thrust magnitude profile, and zero-effort error residuals are used to indicate efficiency and stability of the guidance solutions. Performance in these nominal cases is compared to open-loop optimal solutions. General pseudo-spectral optimal control software (GPOPS) is used to generate the open-loop solutions.

The following techniques were used to determine initial conditions for each dynamical model and to introduce perturbations into the CRTBP and relative motion scenarios.

## 3.1 Halo Orbit Initial Conditions

An iterative process is used to determine the initial conditions of a halo orbit. Specifically, a differential corrections method is employed to compute a periodic orbit. In order to do this it is first necessary to be able to quantify how changes in initial conditions will affect a particle's trajectory in the CRTBP. This is readily accomplished by taking advantage of the linearized variational equations introduced in Section 1.1.3 to create a time-dependent state transition matrix.[7] The following method differs

slightly, however, from the solution presented in Equation 1.37 because the description of variational motion is expanded here to include velocity terms. The new variational term is

$$\delta \mathbf{x} = [\delta x, \delta y, \delta z, \delta \dot{x}, \delta \dot{y}, \delta \dot{z}]^T \quad (3.1)$$

The resulting state space form of the linearized variational equations is therefore

$$\delta \dot{\mathbf{x}} = \mathbf{M}(t)\delta \mathbf{x} \quad (3.2)$$

where

$$\mathbf{M}(t) = \begin{bmatrix} \mathbf{0}_3 & I_3 \\ \mathbf{B}(t) & \mathbf{C} \end{bmatrix} \quad (3.3)$$

Note that although the CRTBP differential equations of motion have been derived to be non-dimensional, for the following explanation time and derivatives with respect to time are given as  $t$  and  $\frac{dx}{dt} = \dot{x}$  rather than  $t$  and  $\frac{dx}{dt} = x'$  in the interest of clarity.

As opposed to the case of linearizing the equations of motion about an equilibrium point as was done in section 1.1.3, the variational equations defined here measure the departure from a reference trajectory rather than a reference point. Therefore, the submatrix  $\mathbf{B}$  is no longer constant and  $\mathbf{M}(t)$  is time-varying.[7] The general form solution to the system in Equation 3.2 is

$$\delta \mathbf{x}(t) = \Phi(t, t_0)\delta \mathbf{x}(t_0) \quad (3.4)$$

where  $\Phi(t, t_0)$  is the state transition matrix. The state transition matrix is a linear map from the initial state at  $t_0$  to some later state at time  $t$ . It is a useful tool in estimating the impact of variations in the initial state on the evolution of the trajectory.[7]

The state transition matrix must satisfy the matrix differential equation[14]

$$\dot{\Phi}(t, t_0) = \mathbf{M}(t)\Phi(t, t_0) \quad (3.5)$$

The state transition matrix can therefore be numerically integrated using Equation 3.5 with the initial condition

$$\Phi(t_{0,0}) = \mathbf{I}_6 \quad (3.6)$$

Since the elements of  $\mathbf{B}(t)$  depend on the reference trajectory, Equation 3.5 must be integrated simultaneously with the CRTBP equations of motion.

The differential correction technique employed here is also known as the multiple shooting method. It is an iterative targeting scheme where the objective is to find the initial conditions that will generate a trajectory that terminates at a given end state or boundary condition.

Halo orbits are symmetric about the  $y = 0$  plane and pierce that plane twice in one orbit. The shooting method uses an initial guess of the state  $\mathbf{x}$  at  $t_0$  and integrates the equations of motion forward in time until the orbit crosses the  $y = 0$  plane, which occurs every one half of an orbit period. The state at the  $y = 0$  plane intersection once propagated forward is of the form

$$\mathbf{x}(t = T/2) = [x_{T/2}, 0, z_{T/2}, \dot{x}_{T/2}, \dot{y}_{T/2}, \dot{z}_{T/2}]^T. \quad (3.7)$$

However, in order for the orbit to be periodic and symmetric its initial state must be of the following form

$$\mathbf{x}(t_0) = [x_0, 0, z_0, 0, \dot{y}_0, 0]^T. \quad (3.8)$$

Due to the periodicity of the orbit, the final state also possesses

$$\mathbf{x}(t_f) = [x_f, 0, z_f, 0, \dot{y}_f, 0]^T. \quad (3.9)$$

The values of  $x_f$ ,  $z_f$ , and  $\dot{y}_f$  are arbitrary, and since the requirement that  $y_f = 0$  is used as a stopping condition for the integrator, the differential corrector only adjusts the initial conditions to drive  $\dot{x}_f$  and  $\dot{z}_f$  to zero.[7]

## 3.2 Halo Orbit Perturbations

Although halo orbits are unstable, it is necessary to add further perturbing forces into the model in order to provide insight into the limits and capability of the optimal sliding guidance algorithm. To do this, the Bicircular Restricted Four-Body Problem is used to incorporate the perturbation of a third primary, in this case the sun, into the Circular Restricted Three-Body Problem. In this model the sun assumed to revolve in a circular orbit around the Earth-Moon center of mass.[25, 14] The equations of motion of the bicircular model are

$$x'' - 2y' = \frac{\partial U_4}{\partial x} \quad (3.10)$$

$$y'' + 2x' = \frac{\partial U_4}{\partial y} \quad (3.11)$$

$$z'' = \frac{\partial U_4}{\partial z} \quad (3.12)$$

where the four-body effective potential is given as

$$U_4(x, y, z, \theta) = U_3(x, y, z) + \frac{\mu_s}{r_3} - \frac{\mu_s}{\rho^2}(x \cos \theta + y \sin \theta) \quad (3.13)$$

Here,  $U_e$  corresponds to Equation 1.35,  $\mu_s$  is the mass of the sun normalized by the mass of the Earth-Moon system,  $\rho$  is the distance between the sun and the Earth-Moon barycenter, and  $\theta$  is the angle between  $\rho$  and the  $x$  axis of the CRTBP rotating frame where  $\theta'$  is the constant angular rate of the sun in this frame. Therefore, the location of the sun is located at any point in time by

$$[\rho \cos \theta, \rho \sin \theta, 0]^T \quad (3.14)$$

Using the previous equation, the sun-spacecraft distance is then calculated to be

$$r_3^2 = (x - \rho \cos \theta)^2 + (y - \rho \sin \theta)^2 + z^2 \quad (3.15)$$

### 3.3 Implementation of Relative Motion Equations

In order to utilize the linearized equations of relative motion and the CWH equations, some kinematic transformations must be applied. Both the chief and deputy orbits are given initially in orbital element descriptions. The following relations are used to convert the orbital element descriptions into state vectors  $\mathbf{x} = [\mathbf{r}, \mathbf{v}]^T$  in the ECI frame. The ECI to LVLH direction cosine matrix is constructed from the unit vector definitions of the LVLH frame

$${}^{\mathcal{N}}\mathbf{h} = {}^{\mathcal{N}}\mathbf{r} \times {}^{\mathcal{N}}\dot{\mathbf{r}} \quad (3.16)$$

$$\begin{aligned} {}^N\hat{\mathbf{o}}_r &= \frac{{}^N\mathbf{r}_c}{r_c} \\ {}^N\hat{\mathbf{o}}_\theta &= {}^N\hat{\mathbf{o}}_h \times {}^N\hat{\mathbf{o}}_r \\ {}^N\hat{\mathbf{o}}_h &= \frac{{}^N\mathbf{h}}{h} \end{aligned} \quad (3.17)$$

$$[ON] = \begin{bmatrix} {}^N \hat{\boldsymbol{o}}_r^T \\ {}^N \hat{\boldsymbol{o}}_\theta^T \\ {}^N \hat{\boldsymbol{o}}_h^T \end{bmatrix} \quad (3.18)$$

This transformation is used to rotate the inertial positions, velocity, and angular velocity vectors into the relative frame. The deputy state in the relative motion frame is therefore given as

$$\boldsymbol{\rho} = {}^\theta \boldsymbol{r}_d - {}^\theta \boldsymbol{r}_c \quad (3.19)$$

$$\dot{\boldsymbol{\rho}} = {}^\theta \dot{\boldsymbol{r}}_d - {}^\theta \dot{\boldsymbol{r}}_c - {}^\theta \boldsymbol{\omega}_{\theta/\mathcal{N}} \times \boldsymbol{\rho} \quad (3.20)$$

where

$$\boldsymbol{\omega}_{\theta/\mathcal{N}} = n \hat{\boldsymbol{o}}_h \quad (3.21)$$

### 3.4 Geospatial Perturbations

The case of relative motion between a chief and deputy spacecraft is perturbed by incorporating a higher fidelity model of the earth's gravitational field. In reality, the earth is an oblate spheroid and not a perfect sphere. In addition, its mass is not uniformly distributed. The restricted two-body problem makes the assumption that the earth can be treated as a point mass. This assumption is valid for most cases and can model the motion of orbiting satellites with an acceptable relative degree of accuracy.

To make the model more realistic, a body's gravitational potential can be expressed as the summation of terms from a spherical harmonic series. The gravitational

potential of the earth is given in this form as[1, 29]

$$U = -\frac{\mu}{r} + \sum_{n=2}^{N_z} \frac{J_n P_n^0(\sin\theta)}{r^{n+1}} + \sum_{n=2}^{N_t} \sum_{m=1}^n \frac{P_n^m(\sin\theta)(C_n^m \cos m\psi + S_n^m m\psi)}{r^{n+1}} \quad (3.22)$$

The details of each term in the this series is beyond the scope of this paper. The first summation comprises what are known as the zonal terms, while the second summation comprises the tesseral terms. The coefficient  $J_n$  in the zonal term summation decreases as  $n$  increases. Thus it is a common practice to approximate Equation 3.21 by only accounting for the zonal term where  $n = 2$  as this is an adequate first order approximation of the effect of the earth's oblateness its gravitational field.

To account for the effect of  $J_2$  gravitational perturbations in the restricted-two body problem, the potential function can be reduced to

$$U(\mathbf{r}) = -\frac{\mu}{r} - R_{J_2}(\mathbf{r}) \quad (3.23)$$

where

$$R_{J_2}(\mathbf{r}) = -\frac{J_2 \mu}{2 r} \left( \frac{R_e}{r} \right)^2 (2\sin^2\phi - 1) \quad (3.24)$$

$$J_2 = 1082.63 \times 10^{-6} \quad (3.25)$$

$$R_e = 6378.15 \text{ km} \quad (3.26)$$

Defining the potential in this way, the acceleration due to  $J_2$  effects can be derived

by taking the gradient of  $U$  with respect to the position vector [1]  $\mathbf{r}$

$$\mathbf{a}_{J_2} = -\frac{3}{2}J_2 \left(\frac{\mu}{r^2}\right) \left(\frac{R_e}{r}\right)^2 \begin{pmatrix} \frac{x}{r} \left(1 - 5\left(\frac{z}{r}\right)^2\right) \\ \frac{y}{r} \left(1 - 5\left(\frac{z}{r}\right)^2\right) \\ \frac{z}{r} \left(3 - 5\left(\frac{z}{r}\right)^2\right) \end{pmatrix} \quad (3.27)$$

and the total acceleration is given as

$$\mathbf{a} = -\frac{\mu}{r^2}\mathbf{r} + \mathbf{a}_{J_2} + \mathbf{a}_C \quad (3.28)$$

In the case of relative motion in low earth orbit, the effect of the perturbing force of the non-spherical nature of the earth's gravitational field is approximately modeled by expressing the acceleration of each satellite independently. The inertial state vectors are then transformed into the LVLH frame at every instant within the control loop.

## 3.5 Control Algorithm

### 3.5.1 Basic Guidance Algorithm

Although the control logic implementation between the CRTBP and relative motion cases differs slightly, the basic control loop algorithm is the same for each. In each case, the scalar differential equations of motion are integrated using the fourth-order Runge Kutta method. A separate control loop calculates ZEM and ZEV, the sliding surface vector differential  $\dot{\mathbf{s}}$ , and ultimately the command acceleration  $\mathbf{a}_C$ . The acceleration is then added into the differential equations of motion to be integrated in the next step of the Runge Kutta function. It is therefore assumed that any commanded acceleration is achieved instantaneously and held at a constant vector for the

duration of the time step. An outer loop controls controls the simulation and allows for the simulation time step, the duration of each burn, and integrator time step to be utilized separately.

In the case of formation flight, this algorithm is used continuously from start to finish. That is, there is no higher control logic dictating the behavior of the guidance algorithm. In each case, the desired end state is zero velocity at the origin of the LVLH frame:  $\mathbf{x}_f = [0, 0, 0, 0, 0, 0]^T$ . The performance of two OGL algorithms are studied in the unperturbed model, and the performance of ZEM/ZEV feedback guidance algorithm with and without sliding augmentation is studied in the perturbed model.

In all cases, the spacecraft is set to have a total mass of 2000 kg with an efficiency parameter  $\alpha = I_{sp}g_0 = 1 \times 10^{-4}$ . Expended fuel mass  $m(t)$  is calculated by numerically integrating the following equation:

$$\dot{m} = -\alpha T \tag{3.29}$$

where  $T$  is the instantaneous thrust magnitude.

### 3.5.2 Stationkeeping Algorithm

In the CRTBP scenario, a more complex control logic is used on top of what has been described in order to perform autonomous stationkeeping in a halo orbit for an indefinite period of time. This algorithm is summarized in Figure 3.1. For stationkeeping, the spacecraft starts out coasting. The controller propagates the CRTBP model equations forward in time by  $d\tau$  to estimate where the spacecraft will be. A reference orbit is used to calculate the point that is closest to the end state of the spacecraft after  $\tau + d\tau$ . Then the distance the spacecraft has deviated off course is calculated by subtracting the position vector of the spacecraft at time  $\tau + d\tau$  from

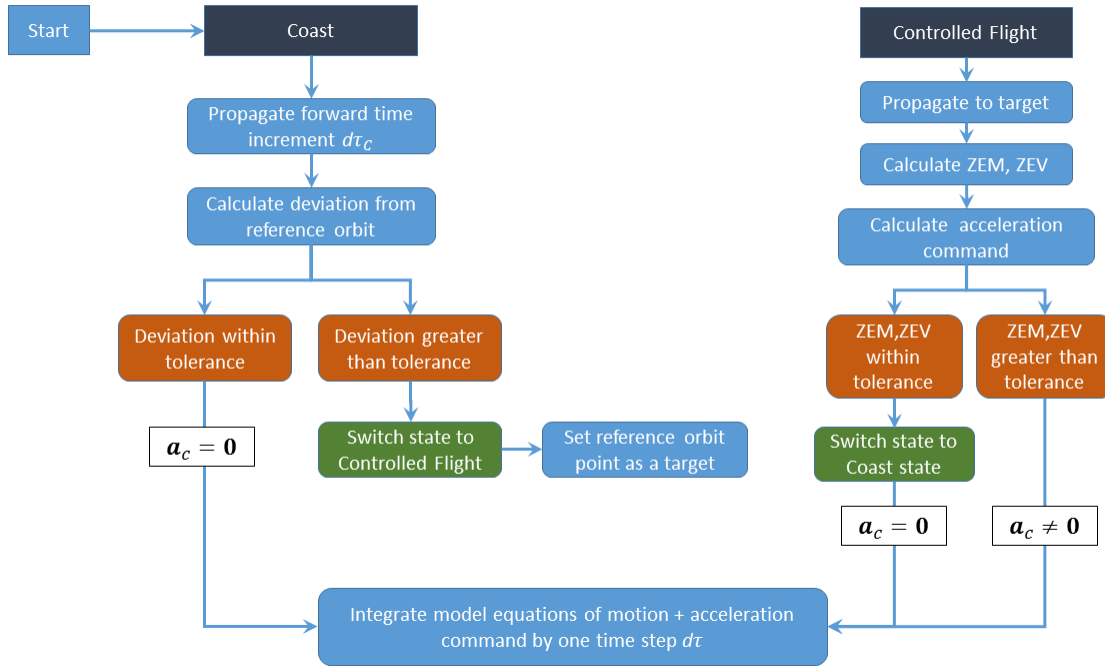


Figure 3.1: Halo Orbit Stationkeeping Guidance Algorithm

the position vector of the reference point. If the deviation is greater than a preset threshold, the control state switched to "Controlled Flight". When this happens, the reference point is then set as a target and guidance law drives the spacecraft to that point on the reference orbit.

The parameter time-to-go,  $t_{go}$  is estimated by determining the time of closest approach to the target if the vehicle were to coast to the target. This can be calculated using MATLAB's ode45.m function set with the end condition to stop at the point when the vector between the spacecraft and the target is perpendicular to the velocity vector of the vehicle, or simply by using knowledge of the reference orbit. Given the initial conditions and period of the halo orbit, it is simple to determine through numerical integration how long it would take for a spacecraft starting at any point on the reference orbit to reach any other point within one orbit. Therefore this time

period can be used as an estimate of time-to-go.

The cases of transfer between two nearby halo orbits and intercept of a moving target in the CRTBP are also explored. For these cases, the simpler controller explained in subsection 3.5.1 is utilized.

# Results

## 4.1 Circular-Restricted Three Body Problem

### 4.1.1 Halo Orbit Station-keeping

The station-keeping algorithm employing both ZEM/ZEV feedback guidance with and without sliding performed as expected in all test cases. The maximum allowable deviation from the reference halo orbit was kept at 1 meter. The deadband was lowered incrementally until a tolerance was reached that could not be achieved by the guidance algorithm. Although a tolerance below 1 meter were achieved, 1 meter was set as an adequate standard. The spacecraft required very little continuous thrust to maintain orbit in the CRTBP model.

A nominal case of OSG applied to the perturbed halo orbit is presented in Figure 4.1. In this figure, the deviation in position and velocity at each point is given, along with ZEM, ZEV, thrust, mass magnitude histories, and a plot of the state space of the sliding-mode term. In Figure 4.1a, the positions and velocity errors show the deviation between the reference halo orbit and OSG-commanded trajectory. The position deviates by a maximum of approximately 50 km and the velocity by approximately 18 cm/s. Figure 4.1b and the ZEM/ZEV residuals indicated that each

target point was successfully reached. For this example, a  $d\tau$  of  $T/3$  was used. That is, the time the guidance algorithm propagated forward to check whether or not the deviation was violated was equal to the orbital period, which for this orbit is 14.7 days, divided by 3. Due to the tightness of the deadband, this essentially forces there to be 3 waypoints positioned equidistantly along the halo orbit.

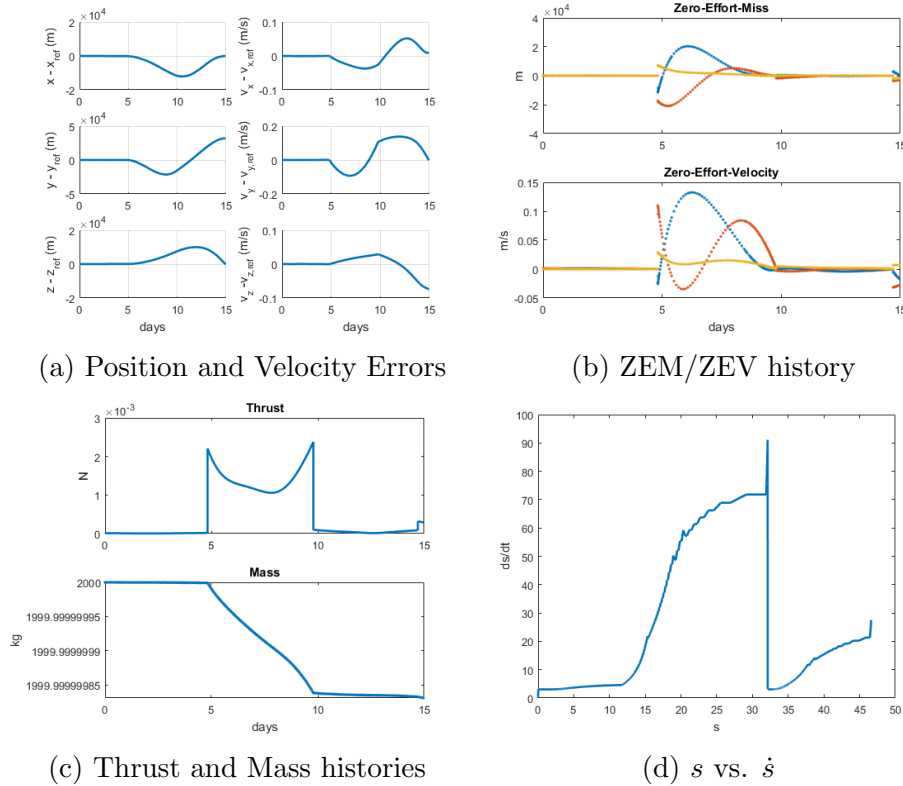
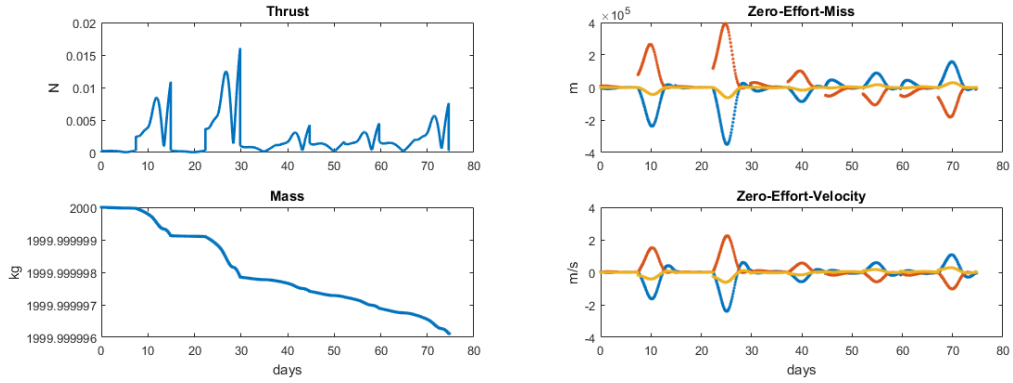


Figure 4.1: Application of OGL as Station-Keeping Solution in Bicircular-Restricted Four Body Problem

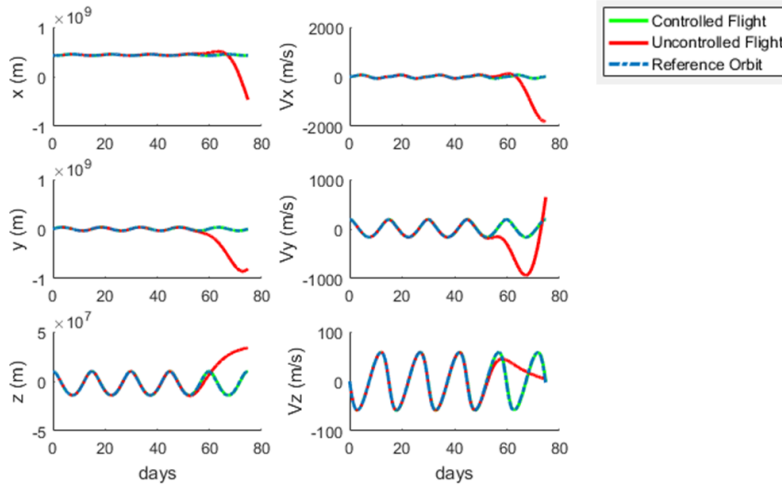
Many studies of the performance of OSG over an extended period of time were performed. The results of one such case is given in Figure 4.2. Here the simulation was run until significant departure was seen from the uncontrolled spacecraft. After 5 orbits, an uncontrolled spacecraft will completely leave the region of the halo orbit. The subplots in Figure 4.2 show the guided spacecraft being continuously corrected with a thrust no greater than 0.02 N to maintain orbit. This stability

held for scenarios in which several years of flight were simulated. Considering, however, the low fuel-cost and matching performance in both the CRTBP model and the perturbed CRTBBP model, the Bicircular Restricted Four-Body Model may not introduce enough of perturbing force to test the robustness of the OSG algorithm in the station-keeping scenario.



(a) Thrust and mass histories

(b) ZEMZEV



(c) Comparison of trajectories

Figure 4.2: Extended station-keeping case in the CRTBP

In order to see the effect of  $n$  on the control algorithm where  $d\tau = T/n$ , it was varied on a the reference orbit over the problem of station-keeping for only one orbit.

The results of this study are given in Table 4.1. Here, the terms  $r_{res}$  and  $v_{res}$  are the integrated position and velocity deviations at each instant over one orbit. They are expressed as

$$r_{res} = \int_{\tau_i}^{\tau_f} r(\tau) d\tau \quad (4.1)$$

$$v_{res} = \int_{\tau_i}^{\tau_f} v(\tau) d\tau \quad (4.2)$$

It can be clearly seen in Table 4.1 that only one target point per orbit, which is identical to setting the initial conditions as the target and spending a time-to-go of  $T$  tracking to the target, is insufficient for station-keeping. The optimal number of waypoints for this particular orbit is 3. For this case, only the OGL controller was tested, as the added sliding-mode term only increases fuel costs. In fact, OGL was shown to be sufficient for all station-keeping scenarios. The sliding-mode term, when implemented, only led to a slightly higher fuel cost. This is expected since sliding-mode control offers robustness at the cost of higher control authority.

$n$	$r_{res}$	$v_{res}$	$m_f(kg)$	$\Delta v_{total}(m/s)$
1	2.96E+09	2.81E+09	4.60E-04	692.2
2.2	1.43E+08	5.14E+07	2.68E-05	62.2
3	4.28E+07	2.88E+07	2.18E-05	68.1
4	2.72E+07	1.99E+07	2.19E-05	74.1
5	2.18E+07	1.71E+07	2.17E-05	63.7
6	2.65E+07	2.50E+07	2.28E-05	67.4
7	2.55E+07	2.06E+07	2.18E-05	63.3
8	1.66E+07	1.35E+07	2.15E-05	64.0
9	8.30E+06	7.12E+06	2.13E-05	60.5
10	1.73E+07	1.46E+07	2.16E-05	62.4

Table 4.1: Waypoint Study in Bicircular Restricted Four-Body Problem

This finding is evident in Figure 4.3 where the results of a parametric study of the parameters  $\Phi$  and  $n$  are varied over a range of values to see the effect on fuel

costs and total integrated position and velocity error. The data show that for greater values of the sliding coefficient  $\Phi$ , which can be thought of as a control gain for the sliding term that is directly proportional to the disturbing acceleration, a higher number of waypoints offers some cost savings. Figure 4.3d depicts the summation of the normalized costs of the other three subplots. It is clear, however, that the optimal set of parameters roughly corresponds to  $\Phi = 0$  and  $n$  less than 6. There are several parameters in this study that are held constant, such as the deadband tolerance and ZEM/ZEV target requirements. Therefore the only other significant take away from this study is that as  $\Phi$  increases, the variance or noise of each of the costs could be seen to be reduced.

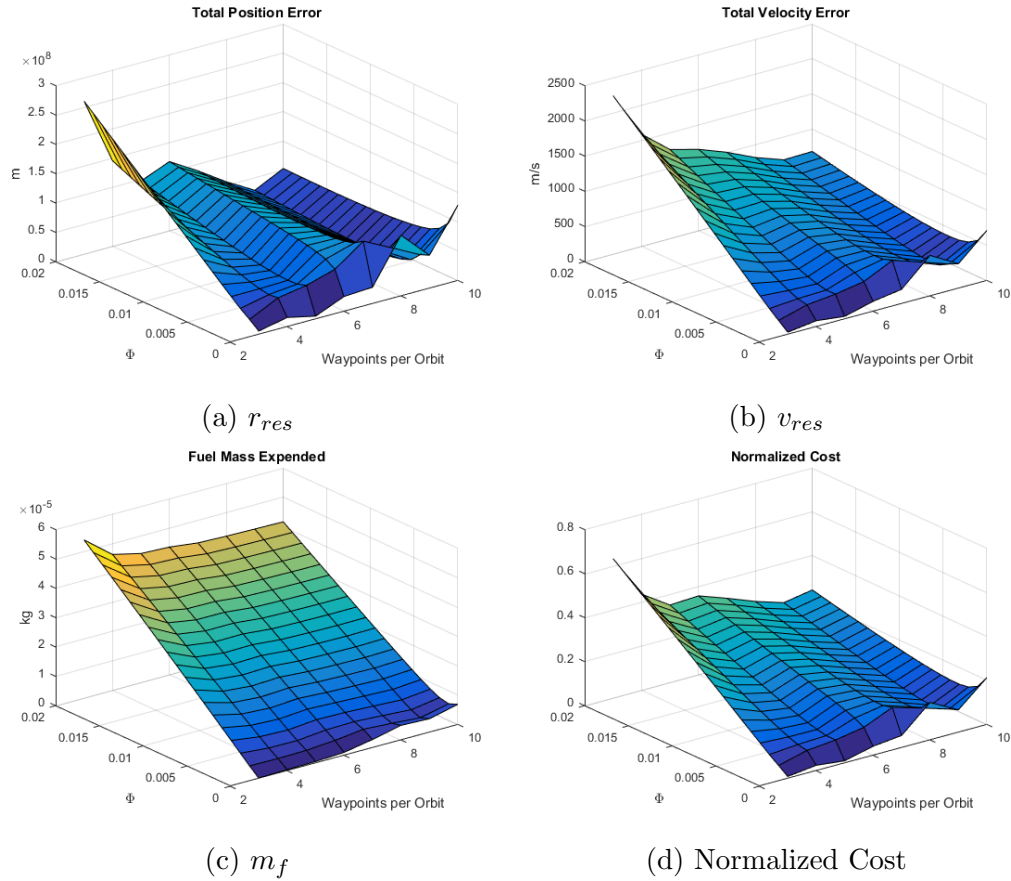


Figure 4.3: Parametric Study of OSG Applied to Station-keeping in the Bicircular Restricted Four-Body model

### 4.1.2 Halo Orbit Transfer

Several scenarios of transfer from the reference halo orbit to a nearby orbit, as well as moving target intercept were conducted. In the case of orbital transfer, between the reference orbit of the previous section and a new, nearby halo orbit, an open-loop solution was created for comparison with OSG. The same initial and target states were used in OSG and the parameter  $\Phi$  was varied to see how well the guidance algorithm performed against the optimal solution. The terminology of this case differs slightly from the station-keeping case in that the final target state is not called a waypoint. A graphical depiction of this scenario is given in Figure 4.4.

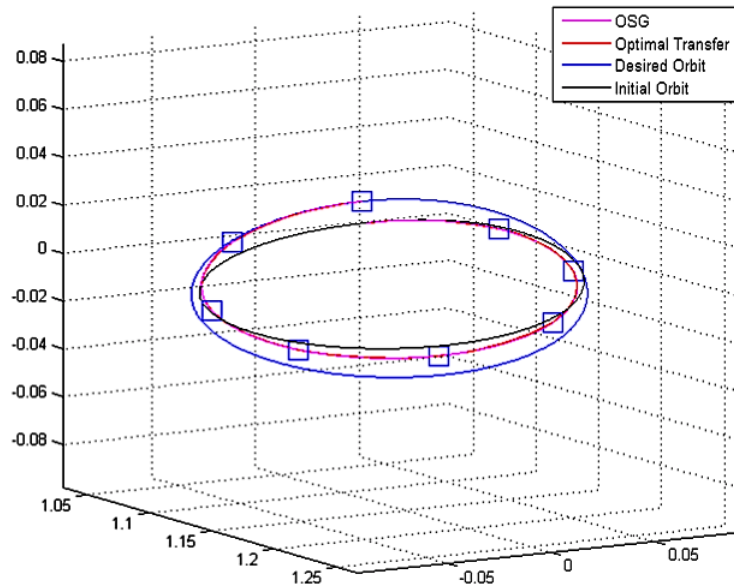


Figure 4.4: OSG Tracking to Optimal Transfer Trajectory Between Two Halo Orbits

It was seen that with a sliding coefficient of  $\Phi = 1 \times 10^{-4}$  gave a solution that cost approximately four times more fuel than the open-loop trajectory, only marginally more than the case in which  $\Phi = 0$ . The results in Table 4.2 show that placing target

waypoints along the optimal continuous thrust trajectory, which has a fuel cost of 3 kg, that the fuel performance of the open-loop solution could be matched. This corroborates Dinius et. al.’s findings that OSG could serve as a valuable addition to any open-loop solution, especially in highly uncertain environments.[12]

Number of Waypoints	0	2	3	5	7
Fuel Cost (kg)	11.42	3.81	3.12	3.02	3.01
ZEM residual (m)	0.97	0.02	0.02	0.03	0.05
ZEV residual (cm/s)	3.24	0.17	0.12	0.16	0.17

Table 4.2: Effect of OSG Waypoints on Optimal Transfer Trajectory

## 4.2 Formation Flight in Low Earth Orbit

In the case of formation flight in low-earth orbit between a deputy and chief satellite pair, the CWH model, LERM model, and J2-perturbed Restricted Two-Body model are used as test cases. First, two the ZEM/ZEV feedback OGL algorithm is compared to an older version of OGL that instead depends on the difference between the spacecrafts current state and target state as feedback input. The latter is termed ” $D_r/D_v$ ” rather than ZEM/ZEV. The  $D_r/D_v$  version of OGL matches D’Souza’s and Battin’s derivations, and thus uses different control gain constants.[3, 2] For this test, the CWH model was used with the orbital elements of both satellites given in Table 4.3. As expected, the ZEM/ZEV version of OGL slightly outperforms the  $D_r/D_v$  version. The trajectories, fuel cost, and thrust profile for this test case are given in Figure 4.5. The  $D_r/D_v$  solution is a more direct trajectory at the cost of slightly higher control effort. Note that for both cases, time-to-go is treated as a fixed value of  $t_f - t_i$ .

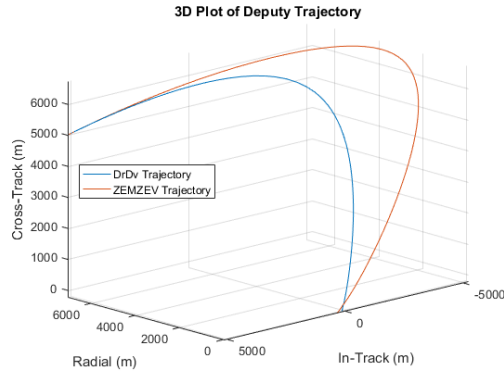
Various researchers have derived a time-to-go function that is designed to calculate

Orbital Element	Chief Satellite	Deputy Satellite
$a$ (km)	7500	7500
$e$ (deg)	0	0.01
$i$ (deg)	45	45.05
$\Omega$ (deg)	20	20
$\omega$ (deg)	30	30
$M_0$ (deg)	20	19.99

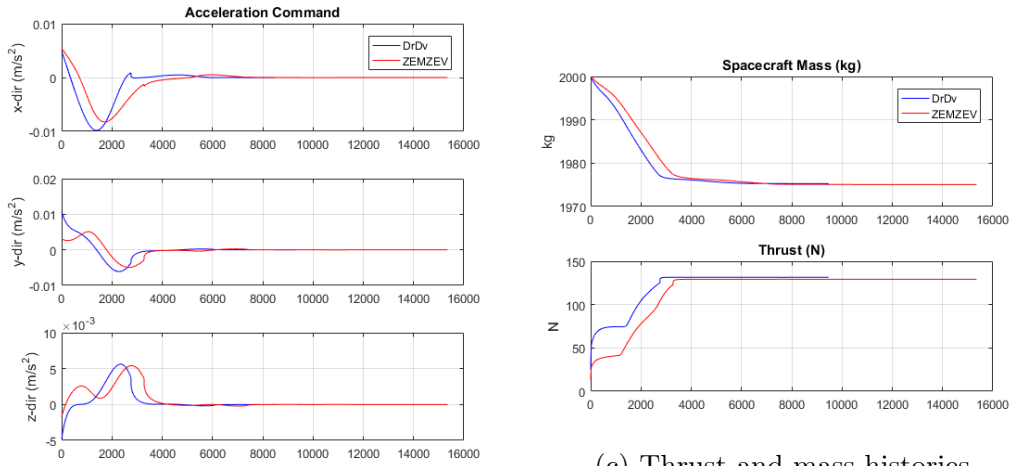
Table 4.3: Initial Conditions for CHW model

the optimal value for  $t_{go}$ . For cases that involve OGL, the transversality condition given in Equation 2.19. is used to express the control Hamiltonian in terms of  $t_{go}$  and can therefore be solved using a root-solving numerical method to find the value of  $t_{go}$  that satisfied the constraint.[3, 13, 15] It was discovered through this investigation, however, that because the transversality constraint also depends on  $\mathbf{g}(\mathbf{r}, t)$ , that in both the relative motion and CRTBP cases this method allowed the nonlinear dynamics to dominate the expression for  $\mathcal{H}(t_f)$ . Through testing it was seen that this method produced erratic and unpredictable results. Therefore in all cases, time-to-go decreases linearly with time. That is, at  $t_i$ ,  $t_{go} = t_f - t_i$ , at  $t_i + dt$ ,  $t_{go}$  now equals  $t_f - (t_i + dt)$ .

A comparison between two optimal open-loop trajectories and OGL is shown in Figure 4.6. The open loop cases include one that is fuel-optimized (discrete control effort) and one that is energy-optimized (continuous control effort). In each comparison, the time-to-go for OGL control was computed using a quartic equation derived from the transversality condition  $H(t_f) = 0$  from D'Souza's original formulation of the optimally controlled lander descent problem[3]. The quartic equation is used to solve for  $t_{go}$  at each instant of the simulation. Although the use of this method provided an accurate solution in this case, it is not expected to generally produce an optimal solution in problems where  $\mathbf{g}$  is not constant. When the assumption



(a) 3-D plot



(c) Thrust and mass histories

(b)  $\mathbf{a}_C$  history

Figure 4.5: Performance of ZEM/ZEV Feedback Guidance vs.  $D_r/D_v$  Feedback Guidance in CHW Model

of uniform gravitation cannot be made, there is no guarantee of optimality. The OGL to open-loop comparisons clearly show that OGL is suboptimal in this test case as OGL incurs approximately 20 kg more in fuel cost to reach the target.

Next, the CHW model was utilized in a parametric study of  $k_R$ ,  $k_V$ , and  $t_{go}$ . Performance for this study was measured only by fuel expenditure. The initial conditions of the deputy and chief orbits are given in Table 4.3. Figure 4.7a shows the surface that corresponds to the optimal value for  $t_{go}$ . Clearly there is a range of values for the

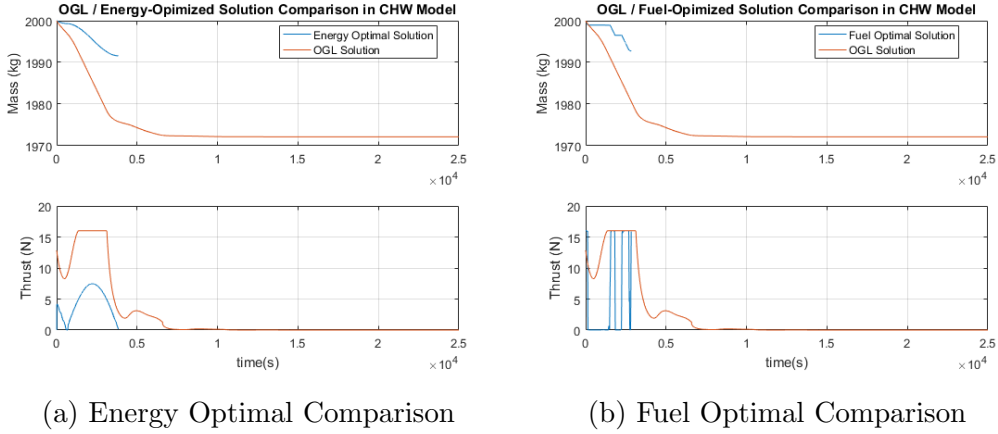


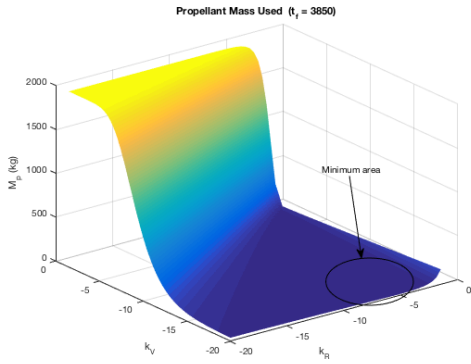
Figure 4.6: Comparison between two optimal solutions computed offline and OGL control gain constants that cause a sharp departure from fuel-optimal performance. The contour plot in Figure 4.7b is a zoomed-in depiction of the 'minimum area' shown in Figure 4.7a.

It is clear that values other than the 6 and -2 for  $k_R$  and  $k_V$  respectively can produce relatively optimal results. This is expected considering that these values are derived from the optimal control problem formulation predicated on the assumption that gravity is uniform. From this parametric study the fuel-optimal parameters are given in the following table.

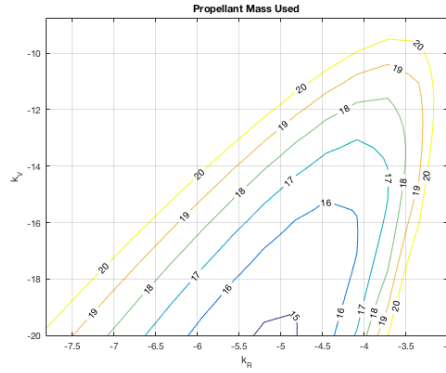
Parameter	Value
Propellant Mass Expended	14.9002 kg
$t_{go}$	3850 seconds
$k_R$	-20
$k_V$	-5.2

Table 4.4: Fuel-Optimal Parameters in LERM Parametric Study

Lastly, the OSG control law is tested in the perturbed Restricted Two-Body model. It was extremely difficult for the algorithm to find a solution when using the initial conditions for the LERM and CWH models. Therefore the deputy's orbit was made identical to the chief's orbit and the eccentricity of the deputy satellites' orbit was



(a) Fuel Cost



(b) Zoomed-in Contour Plot of Fuel Cost Minimum

Figure 4.7: Parametric Study of OSG in LERM Model

Orbital Element	Chief Satellite	Deputy Satellite
$a$ (km)	7500	7500
$e$ (deg)	0	0.01 - 0.075
$i$ (deg)	45	45
$\Omega$ (deg)	20	20
$\omega$ (deg)	30	30
$M_0$ (deg)	20	20

Table 4.5: Initial Conditions for J2-Perturbed Model

gradually increased to test the limits of OGL and to see if OSG could provide improved capability or performance. For all test cases in this study, thrust was limited to 16 N. For cases in which  $\Phi = 0$ , the guidance algorithm could only reach the target state if the deputy orbit eccentricity was less than 0.065. By increasing  $\Phi$  incrementally to a value between 0 and  $1e-3$ , while simultaneously increasing the deputy orbit eccentricity beyond 0.05 to, it was seen that OSG could achieve the target with an acceptable fuel cost (less than 20 kg).

This is demonstrated in Figure 4.8 which shows an instance in which the addition of the sliding-mode term improved the overall fuel cost at the expense of a diminished accuracy for an eccentricity difference of  $\Delta e \approx 0.0693$ . The addition of a sliding-mode

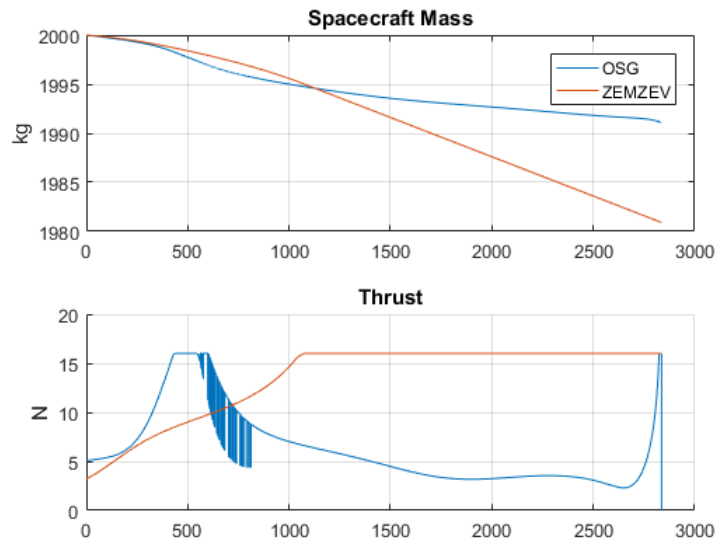


Figure 4.8: Performance of OGL vs. OSG in  $J_2$ -Perturbed Restricted Two-Body Problem

allowed the guidance algorithm to expand the envelope in which it could successfully track to the target from  $\Delta e = 0.06$ . to  $\Delta e = 0.075$ . Note that a success here is measured as a  $ZEM(t_f) < 1$  m and  $ZEV < 1$  cm/s with a fuel cost less than 20 kg.

# Conclusions

In the CRTBP model, OGL remains stable in the perturbed and unperturbed station-keeping problem under tight dead-band constraints. However, the required total  $\Delta v$  per orbit has been found to be nearly an order of magnitude larger than other published station-keeping methods for halo orbits of a similar Jacobi constant [20]. Therefore OGL is not currently a competitive or optimal approach to halo orbit station-keeping. Further study of its performance as a function of halo orbit characteristics such as size, shape, and stability may illuminate ways of improving OGL's performance in this regard. The application of waypoints along a reference orbit was shown to greatly improve performance, with more waypoints incurring a higher control effort but a decreased total deviation from the reference orbit. OGL can serve as an adequate guidance technique to track to the optimal trajectory, as shown in the halo orbit transfer case. The halo orbit station-keeping and optimal orbit transfer test cases corroborate previous findings that ZEM/ZEV feedback guidance works well with waypoint optimization and as a guidance algorithm to track to an open-loop solution. OGL in its current form should therefore not be regarded as a complete solution to autonomous guided flight in the CRTBP, but as a complement to a broader solution.

In the case of spacecraft formation flight in low earth orbit ZEM/ZEV feedback

guidance was shown to outperform an older version of OGL that relied on total position and velocity error instead. Compared to two optimal solutions in the CHW model however, OGL was found to be considerably suboptimal and did not offer a competitive solution. However, it has been shown that the addition of a sliding-mode can expand the capability of OGL in the gravitationally perturbed restricted two-body environment. In this case, stable solutions with reasonable fuel costs were found for problems in which the deputy’s eccentricity was higher than the achievable limit established by using OGL alone. Performance of OGL and OSG appear to depend heavily on parameters  $k_R$ ,  $k_V$ ,  $t_{go}$ , and  $\Phi$ . The parametric studies from both the CRTBP and relative motion scenarios indicate that the control gains  $k_R$  and  $k_V$  and the time-to-go have the potential to improve performance by being tuned to optimal values. One possible avenue of study in this regard is to adaptively tune these parameters through reinforcement learning.

Both the traditional optimal guidance law and the optimal sliding guidance law have been demonstrated to perform suboptimally when compared to optimal open-loop solutions in all CRTBP and relative motion test cases. However, the performance of these algorithms has not yet been exhaustively studied in cases with highly nonlinear dynamics. Several researchers over the past decade have shown that ZEM/ZEV feedback control can be successfully applied to cases outside of the scope of D’Souza’s original powered descent lander problem. In many of these cases, researchers have shown that OGL can be near-optimal in spite of its limitations. In perturbed and unperturbed CRTBP and LEO relative motion cases here, near-optimal performance has not been observed when compared to optimal open-loop solutions. This study has shown, however, that OGL parameters can be tuned to increase fuel-performance and that OSG can still offer practical robust control over OGL in these environments. It has also shown that the addition of waypoints can lead to a more stable and, in

the case of pairing with an open-loop solution, a near-optimal trajectory Future work in this area will involve the application of machine learning to both the placement of waypoints and in creating time-varying parameters,  $k_R$ ,  $k_V$ ,  $t_{go}$ , and  $\Phi$ , in an effort to achieve near-optimality in the same dynamical environments.

# References

- [1] Schaub, H. and Junkins, J., *Analytical Mechanics of Space Systems*, Reston, VA, USA: AIAA, 2009
- [2] Battin, R.H., *An Introduction to the Mathematics and Methods of Astrodynamics*, AIAA Education Series, AIAA, 1987.
- [3] D'Souza, C., "An optimal guidance law for planetary landing", AIAA, 1997.
- [4] Ebrahimi, B., Bahrami., M., and Roshanian, J., "Optimal sliding-mode guidance with terminal velocity constraint for fixed-interval propulsive maneuvers", *Acta Astronautica*, 556-562.
- [5] Zhou, L. and Xia, Y., Improved ZEM/ZEV feedback guidance for Mars powered descent phase, *Advances in Space Research*, 54 (2014), 2446-2455.
- [6] Kirk, D.E., *Optimal Control Theory: An Introduction*. Dover Publications, 2012.
- [7] McInnes, A. "An Introduction To Libration Point Orbits." (2009).
- [8] Davies, K., Parker, J., Butcher, E., "Transfers from Earth to Earth-Moon L3 halo orbits using accelerated manifolds", *Advances in Space Research*. Volume 55, Issue 7, 1 April 2015, Pages 1868-1877.
- [9] Farquhar, R. W., Kamel, A. A., Quasi-periodic orbits about the translunar libration point, *Celestial Mechanics and Dynamical Astronomy* 7 (4) (1973)

- [10] Wie, B., *Space Vehicle Dynamics and Control*, Aiaa, 1998, pp. 282–285
- [11] Ben-Asher, J.Z., I. Yaesh, Optimal guidance with reduced sensitivity to time-to-go estimation errors, *Journal of Guidance, Control, and Dynamics* 20 (1) (1997) 158–163.
- [12] Dinius, J., Furfaro, R., Topputo, F., and Selnick, S., "Near Optimal Feedback Guidance Design and the Planar Restricted Three-Body Problem". 24th AAS/AIAA Space Flight Mechanics Meeting, 2014
- [13] Guo, Y., Hawkins, M, Wie, B., "Applications of Generalized Zero-Effort-Miss/Zero-Effort-Velocity Feedback Guidance Algorithm", *Journal of Guidance, Control, and Dynamics*, Vol. 36, No. 3, May–June 2013.
- [14] Koon, W.S., Lo, M. W., Marsden, J. E., Ross, S. D., *Dynamical Systems, the Three-Body Problem, and Space Mission Design*. 2006
- [15] Guo, Y., Hawkins, M, Wie, B., "Optimal Feedback Guidance Algorithms for Planetary Landing and Asteroid Intercept". *Astrodynamics 2011: proceedings of the AAS/AIAA Astrodynamics Specialist Conference*, 2011.
- [16] Howell, K., "Three-Dimensional, Periodic, Halo Orbits," *Celestial Mechanics*, Vol. 32, No. 1, 1984.
- [17] Hawkins, M. "New near-optimal feedback guidance algorithms for space missions". Doctoral Thesis, Iowa State University, 2013.
- [18] Hill, K. A. "Autonomous Navigation in Libration Points," Doctoral Thesis, University of Colorado, 2007.
- [19] Pavlak, T. A., Howell, K. C., "Strategy for optimal, Long-Term Stationkeeping of Libration Point Orbits in the Earth-Moon System." *Proceedings of the*

AIAA/AAS Astrodynamics Specialist Conference, AAS Paper No. 11-516, August 2012.

- [20] Nazari, M., Anthony, W., and Butcher, E. A., “Continuous Thrust Stationkeeping in Earth-Moon L1 Halo Orbits Based on LQR control and Floquet Theory,” AIAA/AAS Astrodynamics Specialist Conf., AIAA 2014-4140.
- [21] Sherrill, R., Sinclair, A., Sinha, S. C., Lovell, A. “Continuous-Thrust Control of Satellite Relative Motion in Elliptic Orbits using a Lyapunov-Floquet Generalization of the HCW Equations.” AIAA/AAS Astrodynamics Specialist Conference, August 2013.
- [22] Shtessel, Y., Edwards, C., Fridman, L., Levant, A., *Sliding Mode Control and Observation* Springer, New York, 2014.
- [23] Wibben, D., Furfaro, R. ”Optimal Sliding Guidance Algorithm for Mars Powered Descent Phase,” *Advances in Space Research*. Vol. 57, Issue 4, 948-961, February 2016.
- [24] Wibben, D., Furfaro, R., ”ZEM/ZEV sliding guidance for asteroid close-proximity orbital transfer and rendezvous”, 24th AAS/AIAA Space Flight Mechanics Meeting, 2014.
- [25] Mueting, J., Furfaro, R., Toppuo, F., Simo, J., ”Optimal Sliding Guidance for Earth-Moon Halo Orbit Station-keeping and Transfer”, Spaceflight Mechanics 2016, 26th AAS/AIAA Space Flight Mechanics Meeting, 2016.
- [26] Guo, Y., Hawkins, M., Wie, B., ”Waypoint Optimized Zero-Effort-Miss, Zero-Effort-Velocity Feedback Guidance for Mars Landing”, *Journal of Guidance, Control, and Dynamics*, 2013

- [27] Bahrami, M., Ebrahimi, B., Roshanian, J., Optimal sliding mode guidance law for fixed interval propulsive maneuvers, in: IEEE Conference on Control Application, 2006
- [28] Bando, M., Ichikawa, A., Active formation flying along an elliptic orbit, *Journal of Guidance, Control, and Dynamics* 36 (1) (2013) 324–332.
- [29] Vallado, D. A., *Fundamentals of Astrodynamics and Applications* 4th Ed., Microcosm Press. Hawthorne, CA. 2013.